Long-term assessment of airborne radiocesium after the Fukushima nuclear accident: Re-suspension from bare soil and forest ecosystems

M. Kajino[1, 2], M. Ishizuka[3], Y. Igarashi[1], K. Kita[4], C. Yoshikawa[5], and M. Inatsu[6]

[1]{Meteorological Research Institute (MRI), Japan Meteorological Agency (JMA), Tsukuba, Ibaraki, Japan}

[2]{RIKEN Advanced Institute for Computational Science (AICS), Kobe, Hyogo, Japan}

[3]{Kagawa University, Takamatsu, Kagawa, Japan}

[4]{Ibaraki University, Mito, Ibaraki, Japan}

[5]{Japan Agency for Marine-Earth Science and Technology (JAMSTEC), Yokosuka, Kanagawa, Japan}

[6]{Hokkaido University, Sapporo, Hokkaido, Japan}

Correspondence to: M. Kajino (kajino@mri-jma.go.jp)

Abstract

The long-term effect of ^{137}Cs re-suspension from contaminated soil and forests due to the Fukushima nuclear accident has been quantitatively assessed by numerical simulation, a field experiment on dust emission flux in a contaminated area (Namie town, Fukushima prefecture), and air concentration measurements inside (Namie) and outside (Tsukuba city, Ibaraki prefecture) the contaminated area. In order to assess the long-term effect, the full year of 2013 was selected to study just after the start of the field experiments. The ^{137}Cs concentrations at Namie and Tsukuba were approximately $10^{-1} – 1$ and $10^{-2} – 10^{-1}$ mBq/m^3, respectively. The observed monthly median concentration at Namie was one to two orders of magnitude larger than that at Tsukuba. This observed difference between the two sites was consistent with the simulated difference, indicating successful modeling of ^{137}Cs re-suspension and atmospheric transport. The estimated re-suspension rate was approximately 10^{-6} /d, which was

significantly lower than the decreasing rate of the ambient gamma dose rate in Fukushima prefecture (10^{-4} – 10^{-3} /d) as a result of radioactive decay, migration in the soil and biota, and decontamination. Consequently, re-suspension contributed negligibly in reducing ground radioactivity. The dust emission model could reproduce the air concentration of ^{137}Cs in winter, whereas the summer air concentration was underestimated by one to two orders of magnitude. Re-suspension from forests at a constant rate of 10^{-7} /h, multiplied by the green area fraction, could explain the air concentration of ^{137}Cs at Namie and its seasonal variation. The simulated contribution of dust re-suspension to the air concentration was 0.7 – 0.9 in the cold season and 0.2 – 0.4 in the warm season at both sites; the remainder of the contribution was re-suspension from forest. The re-suspension mechanisms, especially through the forest ecosystems, remain unknown. This is the first study that provides a crude estimation of the long-term assessment of radiocesium re-suspension. Additional research activities should investigate the processes/mechanisms governing the re-suspension over the long term. This could be achieved through conducting additional field experiments and numerical simulations.

Keywords: Atmospheric radioactivity, Re-suspension, Dust emission, Unknown re-suspension source, Aerosol, Numerical simulation, Budget analysis, Japan

1   Introduction

The Fukushima Daiichi Nuclear Power Plant (FDNPP) accidentally released nuclear fission products into the atmosphere and the ocean environment following the catastrophic earthquake and tsunami that occurred in March 2011. The accident caused serious contamination of the soil over the Tohoku region (northeastern part of Japan, including Fukushima and Miyagi prefectures) and the Kanto region (eastern part of Japan, including Ibaraki, Tochigi, Gunma, and Chiba prefectures) (NRA, 2012). Since then, a number of studies have been conducted, particularly during the months that followed the accident. These assessments include primary emission estimations (Chino et al., 2011; Danielache et al., 2012; Stohl et al., 2012; Terada et al., 2012; Katata et al., 2012a, 2012b; Winiarek et al., 2012, 2014; Hirao et al., 2013; Saunier et al., 2013; Katata et al., 2015; Yumimoto et al., 2016; Danielache et al., 2016), field observations (ground aerosol sampling: Masson et al., 2011, 2013; Kaneyasu et al., 2012; Adachi et al., 2013; Tsuruta et al., 2014; Igarashi et al., 2015; Oura et al., 2015, aircraft measurements: NRA, 2012, and afoot measurements: Hososhima and Kaneyasu, 2015), and numerical simulations of transport and depositions (deterministic

1   simulation: Chino et al., 2011; Morino et al., 2011; Yasunari et al., 2011; Stohl et al., 2012;

2   Terada et al., 2012; Katata et al., 2012a, 2012b; Winiarek et al., 2012, 2014; Hirao et al.,

3   2013; Saunier et al., 2013; Katata et al., 2015; Yumimoto et al., 2016; Danielache et al., 2016,

4   deterministic simulation with sensitivity runs: Morino et al., 2013; Adachi et al., 2013; Groëll

5   et al., 2014; Saito et al., 2015; Sekiyama et al., 2015; Quérel et al., 2016, uncertainty

6   modeling and probabilistic forecast: Girard et al., 2016; Sekiyama et al., 2016, and multi-

7   model inter-comparison and multi-model ensemble analysis: SCJ, 2014; Draxler et al., 2015:

8   Kristiansen et al., 2016). The targeted radionuclides were species with both short and long

9   half-lives: ^{99}Mo-^{99m}Tc (half-life 65.9 – 6 h), ^{129m}Te (33.6 d), ^{131}I (8.02 d), ^{132}Te-^{132}I (3.2 d –

10   2.3 h), ^{134}Cs (2.07 y), ^{136}Cs (13.2 d), ^{137}Cs (30.1 y), ^{133}Xe (5.2 d), and ^{35}S (87.5 d).

11   In contrast, there have been few studies on the long-term (more than one year) quantitative

12   assessment of radioactivity in the atmosphere associated with the Fukushima accident

13   (Igarashi et al., 2015; Ishizuka et al., 2016; Kinase et al., 2016). More than 100,000 people

14   were evacuated (METI, 2012), and most have still not been able to return to their homes and

15   the public remains anxious about the safety of the affected areas. Radionuclides with long

16   half-lives such as ^{134}Cs (2.07 y) and ^{137}Cs (30.1 y) are of particular concern (Evangeliou et al.,

17   2014). Following the Chernobyl accident there were several studies on the re-suspension and

18   long-term assessment of these radionuclides, such as Holländer and Garger (1996), Garger et

19   al. (1998), Hatano and Hatano (2003) and Garger et al. (2012). For example, Garger et al.

20   (2012) estimated the re-suspension "descending trend" as having a half-life of 300 d based on

21   the surface activity concentration of ^{137}Cs. In the case of the Fukushima accident, Igarashi et

22   al. (2015) estimated the half-reduction time by fitting multi-component exponential functions

23   based on the ^{137}Cs concentration at the Meteorological Research Institute (Tsukuba) as 5.9 d,

24   16 d, and 1.1 y. These estimates were based on the trend in the observed surface air

25   concentrations of ^{137}Cs, and thus the contributions from advection, diffusion, emission and

26   deposition terms were not quantified.

27   There are thousands of monitoring posts situated in the contaminated area in Fukushima

28   prefecture to measure the ambient gamma dose rate. Hoever, the data cannot be used for

29   evaluating internal exposure: evaluation of internal exposure requires direct measurement of

30   the surface air activity concentration. There are only a few observation sites that continuously

31   measure the concentration of radiocesium (e.g., Igarashi et al., 2015; Ishizuka et al., 2016;

32   Kinase et al., 2016). To assess the spatial distribution of the internal exposure hazard, 3D

numerical simulation is necessary to interpolate values for unmonitored locations. The numerical simulation requires emission flux as a boundary condition. However, the mechanism and thus the radioactivity flux associated with the re-suspension of ^{137}Cs were unknown, despite extensive efforts based on field observations (e.g., Igarashi et al., 2015; Ishizuka et al., 2016; Kinase et al., 2016).

Garger et al. (2012) summarized the re-suspension sources following the Chernobyl accident as (1) dust emission, (2) human activity in fields, and on roads and construction sites, (3) forest fires, and (4) emissions from the power plant (i.e., opening of the Chernobyl sarcophagus). Re-suspension sources (1) dust emission (Ishizuka et al., 2016) and (4) i.e., additional emissions from the reactor buildings of FDNPP (TEPCO, 2012; 2013; 2014a; 2014b; 2015) were considered in the present study. With respect to source (2), since Namie town is located in the evacuation zone, human activity has been extremely limited except for decontamination-related work. Although the decontamination-related work could be a potential source of re-suspension, it is not considered in the current simulation as the re-suspension flux has been hardly quantified. As to source (3), there is a low risk of forest fires in Japan given the high humidity although some open biomass burning remains possible. Kinase et al. (2016) found no increase in ^{137}Cs activities when the concentration of levoglucosan, a marker of biomass burning, was increased, and thus re-suspension due to biomass burning was not considered in the present study. In addition to the four sources of ^{137}Cs from the Chernobyl accident, re-suspension from terrestrial biota was considered as suggested by Kinase et al. (2016). They found substantial amounts of bioaerosols upon scanning electron microscopy samples collected in the summer, when ^{137}Cs concentration was high.

In the present study, the long-term effect of radiocesium re-suspension from contaminated soil and terrestrial biota was quantitatively assessed using 3D numerical simulation, a field experiment on dust emission flux in a contaminated area (Namie town, Fukushima prefecture), and air concentration measurements conducted inside (Namie) and outside (Tsukuba city, Ibaraki prefecture) the contaminated area. Even though the re-suspension mechanisms still remain unknown, by utilizing the observational data both inside and outside, together with the transport model, we aimed to provide as a robust analysis as possible of the re-suspension, transport, and re-deposition of ^{137}Cs over the Tohoku and Kanto regions of Japan.

2 Numerical simulation

A brief description of the numerical method, such as the processes considered in the model and simulation settings, are presented in this section, and detailed model formulations are described in Appendix A. Because the schemes and assumptions regarding the emissions are key to the current study, they are described in detail in the following subsections.

2.1 Lagrangian Model and simulation settings

Figure 1 shows the domain of the Lagrangian Model (LM) with model terrestrial elevations, covering 138 – 143 °E and 34 – 39 °N. The model domain covers the southern part of the Tohoku region (the northern mountainous part of the domain, including Yamagata, Miyagi, and Fukushima prefectures), and includes the FDNPP and highly polluted areas such as the Habitation-Restricted Zone (HRZ) (20 – 50 mSv/y) and Difficult-to-Return Zone (DRZ) (> 50 mSv/y) (METI, 2012). It also covers the Kanto region (or Kanto Plain, the largest plain in Japan, approximately 120 km × 120 km), a highly populated region that includes low to moderately polluted areas such as Tokyo, Gunma, Tochigi, Ibaraki, Saitama, and Chiba prefectures.

LM considers horizontal and vertical diffusion and advection, gravitational settling, dry and wet depositions, and radioactive decay. It uses simple parameterizations for dry and wet deposition schemes, and it can be driven by meteorological analysis data sets so that it does not require a meteorological model to predict detailed meteorological fields and variables. The model was designed to be easily handled and computationally efficient so that non-specialists of numerical simulations can conduct long-term assessments of atmospheric diffusion problems using their desktop or laptop computers. The LM was designed for rough budget estimates, as presented in the current study, or for sensitivity analyses using a large number of parameters (e.g., Groëll et al., 2014; Girard et al., 2016; Quérel et al., 2016), rather than for process-oriented analysis (e.g., Morino et al., 2013; Katata et al., 2015) or sensitivity analyses of the physical and chemical parameters of aerosols (Adachi et al., 2013). Details of each process and parameter are described in Appendix A. Statistical error of a Lagrangian simulation is inversely proportional to the square of the number of Lagrangian particles (LPs). The statistical accuracy of the current simulation setting is discussed in Appendix B.

The Grid Point Value Meso-Scale Model (GPV-MSM) of the Japan Meteorological Agency (JMA) was used for meteorological analysis to calculate the transport of LPs. It covers 120 –

1   150 °E and 23 – 47 °N and provides 3 hourly and 16 pressure levels of 3D meteorological

2   variables, from 1000 hPa to 100 hPa, with a horizontal grid resolution of approximately 11

3   km (Δlongitude = 0.125° and Δlatitude = 0.1°) and surface variables at twice the resolution as

4   that for the 3D variables (Δlongitude = 0.0625° and Δlatitude = 0.05°). In the simulation, the

5   whole model domain where LPs can travel is 138 – 143 °E, 34 – 39 °N and from ground

6   surface to 500 hPa. For output of the model results, LP fields are converted to Eulerian

7   concentration (Bq/m^3) and deposition (Bq/m^2) fields in the same horizontal space as the 3D

8   variables but are vertically allocated from the ground surface to an altitude of 1 km at 100 m

9   intervals. The observed surface air concentration was compared with the simulated mean

10   concentration at 0 – 100 m above ground level (AGL).

2.2   Re-suspension from bare soil

12   Ishizuka et al. (2016) developed a re-suspension scheme for radiocesium from bare soil based

13   on measurements on the schoolyard at Namie High School, Tsushima Campus (denoted as

14   Namie (Tsushima) in Table 1 and Fig. 1) in the DRZ.

15   $$F_{soil} = p_{20\,\mu m} F_M (1 - f_{forest}) B_{5\,mm}(t),$$ (1)

16   where F_{soil} is the ^{137}Cs dust re-suspension flux from soil (Bq/m^2/s), $p_{20\mu m}$ is the surface area

17   fraction of dust smaller than 20 μm in diameter against soil containing a maximum size of 2

18   mm particles, and varies depending on soil texture (1.3×10^{-8} for sand, 0.19 for loamy sand,

19   0.45 for sandy loam, and 0.80 for silt loam), F_M is the total dust mass flux (kg/m^2/s), f_{forest} is

20   the forest area fraction, and $B_{5mm}(t)$ is the specific radioactivity of surface soil (from the

21   surface to a depth of 5 mm) (Bq/kg) as a function of time since March 2011. The formula is

22   based on the assumption that dust particles smaller than 20 μm in diameter originated from

23   the surface soil and to a depth of 5 mm were suspended and transported through the

24   atmosphere. The surface area fraction was used for $p_{20\mu m}$ based on the assumption that

25   radiocesium is bound to the surface of soil particles (Evrard et al., 2015). F_M is formulated as

26   being proportional to the cube of the friction velocity u_* (m/s) as described by Loosmore and

27   Hunt (2002) and was applied to the dust emission:

28   $$F_M = 3.6 \times 10^{-9} u_*^3.$$ (2)

29   Since u_* is not available in GPV-MSM, u_* was estimated using a wind speed at 10 m AGL by

30   assuming neutral stratification conditions.

$B_{5mm}(t)$ was derived from the combination of B_{obs}, the observed horizontal distribution of ^{137}Cs deposition obtained from an airborne radiological survey (NRA, 2012) (Bq/m^2) and r_{5mm}, the surface soil activity ratio of 0 – 5 mm to 0 – 5 cm obtained from a vertical profile measurement of ^{137}Cs in the ground soil at Namie High School (= 0.57 Bq/Bq) as

$$B_{5mm}(t) = \frac{B_{obs} r_{5mm} R_{decay}(t)}{5 \times 10^{-3} \rho_{b,soil}}, \tag{3}$$

where $\rho_{b,soil}$ is the bulk density of soil particles per unit volume in the ground space (kg/m^3) obtained from the porosity (0.4 m^3/m^3) and the density of dust particles (2650 kg/m^3). For R_{decay}, which is the decreasing rate of activity in the ground, only radioactive decay was considered for the re-suspension calculation. The decreasing rate due to other processes such as land surface processes (e.g., runoff, erosion, percolation and all the processes resulting in migration of radiocesium in the soil and biota; Evrard et al., 2015; Matsuda et al., 2015) and decontamination were not considered here. Furthermore, suppression of dust emission due to soil moisture and snow cover was not considered. Therefore, it should be noted here that F_{soil} in Eq. (1) is considered as the upper boundary of ^{137}Cs re-suspension flux from surface soil. Effects such as land surface processes, decontamination, and dust emission suppression due to snow cover are extensively discussed in Sect. 5.3 using ambient gamma dose rate measurements obtained by the monitoring posts in Fukushima prefecture.

Eq. (1) is a function of soil texture. The areal fraction of soil texture of the model grid was obtained from the database of the advanced research Weather Research and Forecasting model version 3 (WRFV3; Skamarock et al., 2008). Sixteen categories of soil texture (Miller and White, 1998) with a 30 arcseconds resolution dataset can be obtained from the web after subscription at (http://www2.mmm.ucar.edu/wrf/users/download/get_sources_wps_geog.html, last access: 26 July 2016) and were re-categorized into the above-mentioned four categories (i.e., sand, loamy sand, sandy loam, and silt loam) and interpolated to the LM resolution (~11 km) as shown in Fig. 2a-c. Note that the loamy sand fraction is not presented because it is zero for the entire domain. The parameter f_{forest} (Fig. 2d) was also obtained from the database of WRFV3 and was calculated based on the 24 United States Geological Survey (USGS) Land Use Categories, which are constant over time. The Land Use Category dataset can also be obtained from the above website.

Ishizuka et al. (2016) validated their dust emission module by using a 1D model and observed the surface air concentration of ^{137}Cs at Namie in the winter. After applying the module to our

3D simulation, we found that the air concentration at Namie was underestimated by about factor of five for the same period. The module was formulated based on physical parameters (such as u_*) but contains parameters obtained at a single location (such as r_{5mm} and $\rho_{b,soil}$) and under a fixed atmospheric condition (Ishizuka et al., 2016), whereas ideally parameters in Eqs. (1) – (3) should have considered variations among locations and atmospheric conditions for the 3D simulation. We simply multiplied the dust emission flux by five after adjusting the simulation results against the observed concentration of ^{137}Cs at Namie in the winter. This is one of the simplest top-down approaches for adjusting the emission flux according to the air concentration. The module requires improvement in the future as more reliable parameters become available for various conditions and locations.

2.3   Re-suspension from the forest ecosystems

The re-suspension mechanism of radiocesium from land ecosystems remains unknown. Kinase et al. (2016) found substantial amounts of bioaerosols (rather than mineral dust particles) in samples collected for scanning electron microscopy in the summer, when the ^{137}Cs concentration was high. This does not prove that the bioaerosol was carrying radiocesium, but that it could be a potential carrier. The behavior of Cs in the environment can be inferred by analogy with K, a congener of Cs. Potassium is a necessary and abundant element in plants and circulates between land ecosystems. The addition of potassium fertilizer to a rice field in Fukushima significantly reduced the Cs content of the rice (Ohmori et al., 2014). Substantial amounts of K-salt-rich particles, possibly emitted by active biota such as plants and fungi, and coated with secondary organic aerosols, were observed in pristine Amazonian rainforest (Pöhlker et al., 2012). The major areal fraction of the contaminated area in Fukushima is covered by biota-rich mountain forests. Despite the differences in plant species and locations, it is plausible that water-soluble radiocesium circulating in the biota and soil in the forests was somehow re-emitted into the atmosphere and contributed to the surface air concentration. The re-suspension from the forest ecosystem was simply formulated as follows:

$$F_{forest} = f_{forest} f_{green} r_{const} B_{obs} R_{decay}(t) \,, \tag{4}$$

where F_{forest} is the ^{137}Cs re-suspension flux from forest (Bq/m^2/s), f_{green} and r_{const} are the monthly green area fraction and the constant re-suspension coefficient (/s), respectively, and r_{const} is a tunable parameter to adjust the simulated air concentration of ^{137}Cs to that observed.

1 In the current study, r_{const} is set to 10^{-7} /h by adjusting the simulation data using the
2 observed ^{137}Cs concentration at Namie in the summer, when the re-suspension from soil was
3 negligible due to the higher soil moisture content (following considerable rain) and lower
4 wind speed. As with re-suspension from bare soil, only radioactive decay was considered for
5 R_{decay} and the other processes were not considered. The parameter f_{green} was obtained from the
6 database of WRFV3 and was originally derived from satellite Advanced Very High
7 Resolution Radiometer (AVHRR)/Normalized Difference Vegetation Index (NDVI) data
8 (Gutman and Ignatov, 1998). Whereas f_{forest} remains constant, the monthly averaged f_{green} was
9 used in order to reflect seasonal changes in the activity of the biota.

2.4 Emission from FDNPP (primary emission, additional emissions from the reactor buildings, and unexpected re-suspension associated with debris removal operations)

13 Katata et al. (2015), the Japan Atomic Energy Agency (JAEA)'s latest estimate of the primary
14 emission from FDNPP, was applied for the emergency situation of March 2011, to evaluate
15 the performance of the LM model against the horizontal distribution of ^{137}Cs deposition of the
16 airborne radiological survey (NRA, 2012) (as shown later in Fig. 4a) and surface air
17 concentrations measured at Tsukuba (Fig. 1a). We selected this inventory because it is
18 JAEA's most up-to-date version. Based on an integrated understanding of environmental
19 radioactivity, atmospheric dispersion, and the nuclear reactors, the JAEA team has carefully
20 established a series of inventories for about five years, staring with Chino et al. (2011),
21 followed by Katata et al. (2012a), (2012b), Terada et al. (2012), and finally the current
22 inventory (Katata et al., 2015), which is substantially improved compared to the previous
23 versions.

24 Ongoing emissions during the study analysis period after the emergency situation, that is,
25 January to December 2013, was obtained from the Tokyo Electric Power Co., Inc. (TEPCO)
26 monthly mean emission flux from the reactor buildings (TEPCO, 2012; 2013; 2014a; 2014b;
27 2015). Because only the sum of [134]Cs and ^{137}Cs was provided, the fractions of these two
28 isotopes were calculated based on their half-lives and the assumption that their activities were
29 equal in March 2011 (e.g., Katata et al., 2015), as shown in Fig. 3. The values range from 10^5
30 to 10^7 Bq/h, however for simplicity we set a constant value of 10^6 Bq/h in the current
31 simulation.

1   In August 2013, unexpected re-suspension associated with debris removal operations was

2   reported by TEPCO (2014c) and NRA (2014) and the gross amount was $10^{10} - 10^{11}$ Bq

3   of ^{137}Cs (TEPCO, 2014c, NRA, 2014, Steinhauser et al., 2015). The impact of this unexpected

4   re-suspension is briefly discussed in Sect. 5.2 along with an additional finding, but this

5   emission was not considered in the present LM simulation. In this study we focused on the

6   ongoing and continuous emission, mostly from the natural environment, that is difficult to

7   control.

9   3   Field observations

10   Details of the surface air activity concentration measurement techniques can be found in

11   Ishizuka et al. (2016) and Kinase et al. (2016) for Namie and Igarashi et al. (2015) for

12   Tsukuba. At the both sites, ^{134}Cs and ^{137}Cs surface air concentrations were measured. The

13   sampling intervals were 1 – 2 d at Namie and 1 w at Tsukuba for the analysis period of this

14   study, the year 2013. The observations at Namie started on December 14, 2012, while those at

15   Tsukuba started on March 31, 2003, before the FDNPP accident. In March 2011, the sampling

16   interval was increased at Tsukuba to 6 h – 1 d and the data for these periods were used for the

17   validation of LM and its parameters, as presented in Sect. 4.1.

18   The Namie site is located on the schoolyard of Namie High School, Tsushima Campus, in the

19   Tsushima district of Namie town in Fukushima prefecture, as shown in Table 1 and Fig. 1.

20   Namie town extends from the Hamadori coastal area (denoted as C in Fig. 1) to the Abukuma

21   highland area (B in Fig. 1). There are two sites in Namie town used in the study. In order to

22   distinguish the Tsushima Campus site in the highland area from the monitoring post site

23   located in Omaru district in Namie town in the coastal area, the Tsushima site is referred to as

24   Namie (sometimes as Namie (Tsushima)) and the Omaru site is referred to as Omaru

25   (sometimes as Namie (Omaru)) throughout the manuscript. The Tsukuba site is located on the

26   premises of the Meteorological Research Institute (Table 1 and Fig. 1a).

27   Namie (Tsushima) was located in the DRZ (> 50 mSv/y, ~9.55 μSv/h [1]) and the

28   observed ^{137}Cs deposition amount was 2,300 kBq/m^2 (NRA, 2012). The ambient gamma dose

---

[1] Calculated by the following equation: Annual radiation exposure = (ambient dose rate – background dose rate (=0.04 μSv/h)) × (8 h + 0.4 × 16 h) × 365 d.

1 rate was 11.2 μSv/h on April 1, 2012 at the site and had dropped to 4.8 μSv/h on Feb 16, 2016,

2 and at the HRZ level (20 – 50 mSv/y, 3.85 – 9.55 μSv/h). Tsukuba is located approximately

3 170 km southwest of FDNPP. The observed ^{137}Cs deposition amount was 21 kBq/m^2 (NRA,

4 2012), two orders of magnitude lower than at Namie and the dose rate has remained below 0.1

5 μSv/h since 2012.

4   Results

8 Section 4.1 presents a validation of the LM model and the optimization of the model

9 deposition parameters by using airborne observations (NRA, 2012) and the emission

10 inventory of Katata et al. (2015) for the emergency situation of March 2011. Using the

11 optimized ranges of model parameters validated in Sect. 4.1, the simulated re-suspension

12 of ^{137}Cs from soil and forest, and emission from FDNPP, is presented in Sect. 4.2, and the

13 budgets for re-suspension, transport, and re-deposition are presented in Sect. 4.3.

4.1   Model and parameter validation for the emergency situation (March 2011)

15 Figures 4 and 5 show the observed and simulated distribution of ^{137}Cs deposition in March

16 2011, and the scatterplot comparing the observational and simulation results. In the simulation

17 shown in the figures, the "reference" sets used for dry and wet deposition parameters, namely,

18 the collection efficiency of aerosols using hydrometeors E_c (Eq. A2) and the dry deposition

19 velocity over land v_d (Eq. A4), were 0.04 and 0.1 cm/s, respectively.

20 Since LM uses simple parameterizations for dry and wet deposition, as described in Appendix

21 A, sensitivity tests were conducted for model validation, together with optimization of the

22 deposition parameters. Table 2 summarizes the ranges of the deposition parameters for the

23 sensitivity tests and the results of the ^{137}Cs budget and statistical measurements between the

24 observations and the simulation.

25 The parameter E_c was 0.05 for the JMA dispersion model (JMA, 1998) but the targeted

26 species are different. For example, volcanic ash (particles larger than 1 μm in diameter) used

27 for the JMA model were generally larger than the aerosols carrying ^{137}Cs (around 1 μm in

28 diameter observed in the downwind area, Tsukuba, Kaneyasu et al. 2012, Adachi et al., 2013).

29 Since the inertia of these smaller ^{137}Cs particles is likely to be smaller than that for volcanic

30 ash, E_c could be smaller. The range of E_c was set as 0.02 – 0.06. The dry deposition velocity

1   v_d was selected as 0.1 cm/s for ^{137}Cs in Furuno et al. (1999). The range for v_d was set as 0.05

2   to 0.15 in the present study.

3   The emission inventory of Katata et al. (2015) amounted to 14.1 PBq from March 12 to April

4   1, 2013. The simulated deposition over the model domain (138 – 143 °E, 34 – 39 °N) ranged

5   from 3.4 – 4.7 PBq, which is approximately 24 – 33 % of the emission from the FDNPP.

6   Sixty percent of the total deposition occurred over land, for a total of 2.0 – 2.8 PBq, which is

7   close to the observed value of 2.68 PBq, and the observed value is within the range of the

8   sensitivity runs. Statistical measures such as the fractional bias FB, the correlation coefficient

9   R (linear vs. linear), and FAx (fraction of the simulated values within a factor of x) are listed

10   in Table 2. To find better combinations of (or to optimize) the dry and wet deposition

11   parameters, sensitivity runs were screened based on the criteria $FA10 > 0.9$, $FA5 > 0.7$, $R >$

12   0.75, and an absolute value of $FB < 10\%$. Only one combination $(E_c, v_d) = (0.04, 0.1$ cm/s$)$

13   satisfied the criteria, and thus this is referred to as the "reference" parameters. To evaluate the

14   sensitivity (or uncertainty) of the re-suspension simulation for 2013 due to the deposition

15   parameters, the range of the combination of parameters was set as $(E_c, v_d) = (0.03 – 0.05,$

16   $0.05 – 0.1$ cm/s$)$ around the reference parameters (referred to as the "optimized range") by

17   excluding the parameters with the worse performances. The ranges of the statistical measures

18   of the optimized runs are listed in Table 2. FB, R, $FA2$, $FA5$, and $FA10$ after the optimization

19   had the ranges -0.18 – -0.036, 0.74 – 0.77, 0.26 – 0.30, 0.68 – 0.74, and 0.91 – 0.92,

20   respectively. These statistical measures were comparable to those reported in previous multi-

21   model comparison studies (R: 0.27 – 0.85, FB: -0.84 – 0.56, and $FA2$: 0.14 – 0.57, in SCJ,

22   2014 and Draxler et al., 2015). The current model is thus shown to be sufficiently credible for

23   the budget analysis in this study, despite the simple parameterization and the low resolution in

24   space (~11 km) and time (3 h).

25   In agreement with many previous studies, the simulated contribution of wet deposition was

26   larger than that of dry deposition: the ratio of the amount of dry to wet deposition ranged from

27   0.12 – 0.23 for the optimized parameter ranges, indicating that the results were less sensitive

28   to the dry deposition parameter. Generally speaking, R became higher as E_c became lower,

29   whereas FAx became higher as E_c became higher for the various ranges of the sensitivity tests.

30   Therefore, lower E_c did not meet the criteria of FAx and higher E_c did not meet the criteria of

31   R. Consequently, after the optimization, the maximum values of the statistical measures were

32   lower but the minimum values became higher, indicating that the optimization was successful

1   in excluding the parameters with the worse performances (rather than selecting the best

2   parameters). It should be noted here that the optimized deposition parameters are not

3   necessarily physically valid but rather give simulation results consistent with the available

4   observations. The results presented in this section indicate that the current LM simulation

5   with these optimized parameters has the potential to reproduce consistent features of the

6   radiocesium budget over the Tohoku and Kanto regions of Japan.

7   Figure 6 shows the temporal variation of simulated (red) and observed (black) ^{137}Cs

8   concentrations at Tsukuba in March 2011. The model reproduced the three major plumes

9   arriving at Tsukuba on March 15-16, 20-21, and 28-30; a plume on March 23 was not

10   observed but only appeared in the simulation. The red shaded areas indicate the range of ^{137}Cs

11   concentrations obtained when the simulations were run using the optimized parameter ranges

12   $E_c = 0.03 – 0.05$ and $v_d = 0.05 – 0.1$ cm/s. Due to differences in the parameters used, the

13   surface air concentration could vary by approximately one order of magnitude in transported

14   plumes that experienced wet scavenging along their pathway.

15   **4.2   Re-suspension in 2013**

16   Figure 7 shows the observed and daily mean simulated (with the reference parameters)

17   surface air concentrations at Namie and Tsukuba for the year 2013. The red, green, and blue

18   lines indicate re-suspension from soil, re-suspension from forest, and emission from the

19   FDNPP reactor buildings, respectively. Scatterplots between the observed and the simulated

20   total concentrations are also shown in the figure and the statistical measures between them are

21   listed in Table 3. The correlation coefficients (linear vs. linear) are low at the both sites, but

22   the simulated and the observed medians are close with each other and *FAx* show high values

23   at the both sites. Consequently, the current simulation is enough credible for the quantitative

24   assessment of the annual radiocesium budget.

25   As discussed in Sect. 2.2, note that the re-suspension flux due to the dust emission module

26   (Ishizuka et al., 2016) is multiplied by five in this study in order to adjust to the observation

27   level at Namie in the cold season (January to March, October to December). Also note that

28   the re-suspension coefficient r_{const} in Eq. (4) was set as 10^{-7}/h in order to adjust to the

29   observation level at Namie in the warm season (May to September). The emission flux

30   reported by TEPCO varied from 10^5 to 10^7 Bq/h during the study period but we set it to 10^6

31   Bq/h for simplicity. We did not try to precisely adjust r_{const} to the observation by, for example,

1   using inverse modeling, and instead we simply multiplied by power-of-ten values (except for

2   dust emission, which is five), which are constant in time and space because (1) this facilitated

3   straightforward interpretation of the simulation results by keeping the simulated variation

4   solely originating from the variation of boundary conditions (i.e., emission and meteorology),

5   and therefore (2) this provided simple but useful hints for understanding the re-suspension

6   mechanisms, which remain unknown.

7   Using the dust emission module (which has a physical basis), ^{137}Cs flux re-suspended from

8   soil could account for the level of the observed surface air concentration of ^{137}Cs at Namie in

9   the cold season. Under the influence of the northwesterly winter monsoon, the surface wind

10   speed is high over the contaminated area compared to the summer (as shown later in Fig. 10).

11   Note that the flux might be a maximum estimate since it does not consider land surface

12   processes (such as soil moisture, snow cover, or migration of ^{137}Cs in the soil and biota) and

13   decontamination, which could reduce the ^{137}Cs re-suspension flux. In contrast, in the warm

14   season, the estimated flux significantly underestimated the observation by one to two orders

15   of magnitude due to the weak surface wind, indicating that the dust emission process may not

16   be the sole process involved in sustaining the air concentration of ^{137}Cs during this period.

17   Introducing the ^{137}Cs re-suspension component from forest with a resuspension coefficient of

18   10^{-7}/h and a monthly variation in the green area fraction (derived from NDVI) could

19   quantitatively account for the observed air concentration together with its seasonal variation at

20   Namie. Even though both the simulated re-suspension from soil and forests reproduced the

21   quantity and seasonal variation of the background concentration (in other words,

22   concentrations originating from continuously presenting emissions, such as natural emissions,

23   and not accidental ones) at Namie, sporadic peak events, such as the daily mean ^{137}Cs

24   concentration exceeding 10 mBq/m^3 as observed in June and August at Namie, were not

25   simulated. Some specific re-suspension events might occur from the highly contaminated

26   areas such as the premises of FDNPP (e.g. debris removal operations) or very close to FDNPP

27   on these days, as indicated later in Sect. 5.2. The simulated ^{137}Cs concentrations due to the

28   monthly mean emission from the reactor buildings (=10^6 Bq/h) significantly underestimated

29   the observed concentration by more than three orders of magnitude at Namie and by two

30   orders of magnitude at Tsukuba. Even the maximum estimate of 10^7 Bq/h does not reach the

31   observed level. The emission from FDNPP may not have been the sole process sustaining the

32   air concentration of ^{137}Cs in 2013, supporting the discussion in Igarashi et al. (2015), which

concluded that direct emission from the FDNPP played a minor role in the observed atmospheric radiocesium concentrations over Tsukuba during 2013-2014.

The observed air concentration of ^{137}Cs at Tsukuba was about one to two orders of magnitude lower than that at Namie. The simulated difference between the two sites inside and outside of the contaminated areas was consistent with the observed difference. This finding indicates that the current LM simulation provided consistent features of re-suspension, transport, and re-deposition in the Tohoku and Kanto regions of Japan of ^{137}Cs originating from Fukushima.

4.3 Budget analysis

Figure 8 illustrates the simulated (with the reference parameters) annual amounts of total re-suspension and re-deposition of ^{137}Cs, together with their ratios to the observed deposition (Fig. 4a). The simulated areal total re-suspended amount was 1.28 TBq, which was equivalent to 0.048% of the total deposited amount, 2.68 PBq. The areal total re-deposited amount (with the reference parameters) was 0.22 TBq (0.18 – 0.23 TBq for the optimized range of the deposition parameters), corresponding to approximately 17.2 (14.1 – 18.0) % of the re-suspended amount deposited mainly in the Tohoku region, with the remainder being transported out of the model domain. Therefore, the regional mean rate in the decrease of the land surface ^{137}Cs concentration due to re-suspension was estimated to be 0.040 (0.039 – 0.041) %/y^2, equivalent to 1.1 (1.06 – 1.12) $\times$ 10^{-6} /d. The spatial distribution of the re-suspension and re-deposition ratio to the primary deposition ranged from 0.01 – 0.3% and 0.001 – 0.03%, respectively. The spatial distribution of the land surface ^{137}Cs deposition decay due to re-suspension ranged from 2.7×10^{-7} – 8.2×10^{-6} /d. Re-suspension therefore had a negligible effect on reducing land surface radioactive contamination.

5 Discussion

Seasonal variation of the surface activity concentration and its source contributions are extensively discussed in Sect. 5.1. A possible source of the observed sporadic peak events, which could not be reproduced by the simulation, is discussed in Sect. 5.2. The effects of

---

^{2} The amount re-suspended, excluding re-deposition (1.28 TBq minus 0.22 (0.18 – 0.23) TBq) for the year 2013, divided by the total deposited amount of 2.68 PBq.

1 other processes that were not considered in the model, such as land surface processes and

2 decontamination, are discussed based on the dose rate measurements from the monitoring

3 posts in Fukushima in Sect. 5.3. Future issues are summarized in Sect. 5.4.

4 5.1 Seasonal variation and source contribution

5 The discussion in this section expands on that in Sect. 4.2. Figure 9 shows the same temporal

6 variation as Fig. 7 but for simulated (using the optimized ranges of parameters) results

7 for ^{137}Cs from dust and FDNPP in winter (January to March) and from forest and FDNPP in

8 summer (June to August).

9 In the winter, the simulated trend for dust agreed well with the observed trend (Fig. 9a), and

10 the surface air concentration during this period was positively correlated with the surface

11 wind speed in both the simulation ($R = 0.88$ on hourly basis) and the observations ($R = 0.32$

12 on daily basis). There was a sporadic peak in the observational data of 6.7 mBq/m^3 from the

13 March 17 at 13:00 local time (LT) to March 18 at 13:00 LT that could not be reproduced by

14 the dust module, and this peak coincided with a plume arriving from FDNPP, as shown in Fig.

15 9c. Therefore, the observed peak could be accounted for by specific re-suspension events on

16 the order of 10^9 Bq/h (the left axis divided by the right axis multiplied by 10^6 Bq/h in Fig. 9c)

17 if they occurred on the premises of FDNPP or close to the area. There are also two events

18 exceeding 2 mBq/m^3, one in January and another in February. It is unlikely that the two peaks

19 originated from the direct emission from FDNPP and likely that they originated from the dust

20 emission because the observed peaks coincided with the simulated dust peaks (Fig. 9a) and

21 not with the simulated peaks due to the FDNPP emission (Fig. 9c).

22 In the summer, the simulated quantity as well as the variation in the forest data agreed well

23 with the observed data (Fig. 9b). Because there is only monthly variation in the simulated

24 emission, the simulated daily trend solely originated from variations in the meteorological

25 parameters (wind field, turbulent mixing, and wet scavenging). A significant peak of 60.4

26 mBq/m^3 is observed from August 14 at 13:00 LT to August 15 at 13:00 LT. This observed

27 level was approximately two orders of magnitude larger than the simulated level and one to

28 two orders of magnitude larger than the observed level for the other days in this period.

29 Therefore, continuous emission such as re-suspension from forest is less likely to be the

30 origin of the peak. Because the observed peak and the simulated peak of ^{137}Cs from FDNPP

31 coincided (Fig. 9d), the observed level could be accounted for by specific re-suspension

1   events on the order of 10^{10} Bq/h either on the premises of FDNPP or close to the area. There

2   have been several arguments that the observed peaks in August 2013 were associated with

3   debris removal operations at FDNPP and this is discussed separately in Sect. 5.2.

4   Figure 10 illustrates the seasonal mean surface wind vector and surface air ^{137}Cs

5   concentration (simulated using the reference parameters) due to (a) dust re-suspension in the

6   winter and (b) forest re-suspension in the summer. Due to the prevailing northwesterly winter

7   monsoon, ^{137}Cs was carried southeastward in the winter. In the summer, under the influence

8   of the Pacific high pressure system, ^{137}Cs was carried inland. The monthly mean wind speed

9   is high in winter and low in summer. The upper panels of Fig. 11 illustrate the observed and

10 simulated (using the optimized ranges of parameters) total (from soil, forest, and

11 FDNPP) ^{137}Cs concentration at Namie and Tsukuba. The time resolutions of the simulation

12 are daily for Namie and weekly for Tsukuba to be consistent with the sampling intervals of

13 the two respective sites. The simulation successfully reproduced the quantity and variation in

14 the observed background concentration at Namie and Tsukuba but could not reproduce the

15 sporadic peak events observed at Namie, as discussed above. The simulation also significantly

16 underestimated the observations at Tsukuba from January to March, 2013. Due to the

17 northwesterly monsoon (Fig. 10a), there was less air mass transported from FDNPP to

18 Tsukuba in the winter and therefore this underestimation is probably due specifically to

19 underestimation of the simulated re-suspension around Tsukuba. The lower panels of Fig. 11

20 show the relative contributions of ^{137}Cs from soil and forests at Namie and Tsukuba. The

21 contribution from FDNPP was negligible throughout the year. At both sites, the contribution

22 from dust was high (0.7 – 0.9) in the cold season and low (0.2 – 0.4) in the warm season due

23 to higher surface wind speed in the cold season.

24 Figure 12a shows the observed and simulated (with the reference parameters) monthly Namie

25 to Tsukuba ^{137}Cs concentration ratios. The mean concentration ratio exceeded 100 in June and

26 200 in August due to the sporadic peak events. The monthly median would be relevant for

27 comparing the background observation with the simulation results by considering only

28 continuous emission sources. The values of the simulated concentration ratio and its seasonal

29 variation agreed fairly well with the observed monthly median ratio: the observed and

30 simulated annual means were 38.9 and 31.1, respectively. Fig. 12b shows the monthly mean

31 simulated re-suspension source area contributions to the ^{137}Cs air concentration at Namie and

32 Tsukuba. The re-suspension source area is defined as the model grid where the observed

deposition amount exceeded 300 kBq/m^2 (Fig. 4a) and includes the Namie grid (2,300 kBq/m^2). Eighty to 90% of the ^{137}Cs air concentration at Namie originated from the source region, and there was no clear seasonal variation in the value. In contrast, Tsukuba is characterized as a downwind region and there was clear seasonal variation in the source contribution ratio: high in summer and low in winter, due to the summer and winter monsoons, as discussed above. Nonetheless, the highest value at Tsukuba was 0.4 in July, and so more than half of the ^{137}Cs concentration at Tsukuba originated locally or from areas other than the contaminated regions throughout the year. As shown in Figs. 11a and 11b, the variability in the simulated concentration at Tsukuba due to uncertainty in the deposition parameters was much larger than that at Namie. The differences in the variability indicated that the Namie and Tsukuba sites can be characterized as the source area and the downwind area, respectively: as the time required for the plume to move from the emission site to the observation site increases, the variability becomes larger due to the increased chance for the plume to experience dry and wet scavenging.

5.2 Possible source of sporadic peak events

There have been several scientific studies and governmental reports on the unexpected re-suspension from FDNPP in August 2013. The high dose rate alarm was activated on August 19 within the premises of FDNPP associated with the debris removal operation. Matsunami et al. (2016) related the radiocesium contamination of brown rice in Fukushima in 2013 to this operation, whereas MAFF (2015) denied any association. The NRA estimated the ^{137}Cs emission rate during the debris removal operation as 6.7×10^{10} Bq/h and the cumulative amount as 1.1×10^{11} Bq (NRA, 2014). TEPCO (2014c) estimated the emission rate during the operation as 5.8×10^{10} – 1.2×10^{11} Bq/h and the cumulative amount as 1.3 – 2.6×10^{11} Bq. Steinhauser et al. (2015) estimated the gross amount as 2.8×10^{11} Bq using measurements of weekly air filter sampling and monthly deposition, and a numerical simulation. Their estimates are of the similar order of magnitude as our estimate (10^{10} Bq/h, see Sect. 5.1) but the dates are different: our observed peak was earlier than the reported removal operation.

Our daily sampling showed a peak concentration (60.4 mBq/m^3) from August 14 at 13:00 LT to August 15 at 13:00 LT before the reported operation, but did not detect high concentrations in the August 19 (0.33 mBq/h for August 18 at 13:00 LT to August 19 at 13:00 LT and 1.2 mBq/h for August 19 at 13:00 to August 20 at 13:00 LT). Figure 13 shows the forward trajectories predicted by the LM (statistical locations of LPs) starting from FDNPP on August

14 (left) and August 19 (right). The sky-blue lines and red dashed circles indicate areas
containing approximately two-thirds of the LPs within 1 km AGL: the extent of the area
reflects horizontal and vertical atmospheric diffusion. The highest dose rate peaks were
observed from 13:50 LT to 14:10 LT on August 19 at 2.8 – 8.3 km north and north-northwest
of FDNPP on the leeward side, as reported by Fukushima prefecture
(https://www.pref.fukushima.lg.jp/download/1/20130827moni.pdf.pdf, last access: 26 July
2016). The forward trajectories on August 19 indicated that plumes during the debris removal
operation traveled north-northwest to north of FDNPP (Figs 13b and 13d), rather than towards
the west-northwest where the Namie site is located. On August 14, on the other hand, plumes
were transported towards the west (starting at 12 LT, Fig 13a), and then to the north (starting
at 15 LT, Fig. 13c) due to fast changes in wind direction, resulting in the simulated peak
concentration shown in Fig. 9d during this period. Our simulation and observations together
indicated that the same order of magnitude of ^{137}Cs emission occurred on August 14 – 15 and
on August 19. Alarm activation was not reported on August 14 – 15 but debris removal
operation was also conducted on August 14 and 16 (MAFF, 2015).

5.3 Land surface processes, decontamination, and dust emission suppression due to snow cover

Figure 14 presents the time series of ambient gamma dose rates measured at the monitoring
posts in Fukushima prefecture indicated in Fig. 1b. The data were obtained from the Nuclear
Regulation Authority (NRA), Japan website (http://radioactivity.nsr.go.jp/map/ja/index.html,
last access: 26 July 2016). A total of six, two of the monitoring posts from three geographical
areas (Hamadori coastal area, Abukuma highland area, and Nakadori valley area), were
selected. There are tens to hundreds of monitoring posts in each municipality (village, town,
and city) in Fukushima prefecture. We selected a monitoring post in each municipality by
applying the following conditions: a post showing the highest dose rate of all posts in the
municipality at the time of downloading (around 11:00 a.m., December 28, 2015), data are
available since April 1, 2012, and the instruments are situated 100 cm above the ground.

The government of Japan designated the evacuation-directed zones as a Difficult-to-Return
zone (DRZ) (> 50 mSv/y; 9.55 μSv/h), a Habitation-Restricted Zone (HRZ) (20 – 50 mSv/y;
3.85 – 9.55 μSv/h), and a zone being prepared to have the evacuation directive lifted (< 20
mSv/y; 3.85 μSv/h), in April 2012 (METI, 2012). The two sites in the Hamadori area, Okuma
and Omaru, have been designated DRZ (13.6 and 11.8 μSv/h on December 28, 2015). The

1 dose rates at the two sites in the Abukuma area, Iitate and Kawamata, dropped below the HRZ

2 level during the analysis period in this study (1.17 and 0.521 μSv/h on December 28, 2015).

3 The dose rates in the Nakadori area are below 1 μSv/h (0.242 and 0.201 μSv/h on December

4 28, 2015).

5 The dose rate significantly dropped when the ground was covered with snow, in January and

6 December 2013 in Hamadori and Nakadori, and from January to early March and December

7 2013 in Abukuma (the elevation of Abukuma is 500 – 1,000 m and higher than Hamadori and

8 Nakadori). Snow cover suppresses re-suspension due to dust emission. Namie (Tsushima) is

9 located in Abukuma and the ground was covered with snow until early March (Ishizuka et al.,

10 2016). The observed air concentration of ^{137}Cs at Namie (Tsushima) was correlated with the

11 wind speed in the winter from January to March, indicating that re-suspension during the

12 period was mechanically induced. In the winter, dust re-suspension from outside Abukuma,

13 such as from Hamadori and Nakadori, or from land surface where the snow cover was partly

14 melted due to solar radiation, might be the dominant source contributing to the ^{137}Cs surface

15 air concentration at Namie (Tsushima) when the ground was covered with snow.

16 The first order decreasing rates fitted by the least-square approximation for the period without

17 snow cover, May to October 2012 and 2013, are presented in Fig. 14. The rates ranged from

18 5.2 – 12.1 ×10^{-4} /d. The monthly mean radioactive decay rates of total radiocesium (^{134}Cs

19 + ^{137}Cs), determined by assuming that the activities of ^{134}Cs and ^{137}Cs were equivalent in

20 March 2011, were 4.2×10^{-4} /d and 3.0×10^{-4} /d in April 2012 and March 2014, respectively,

21 due to the difference in half-life of ^{134}Cs and ^{137}Cs (2.07 y and 30.1 y, respectively). By

22 assuming that the gamma dose rate primarily originated to radiation from the land surface

23 radiocesium, the radioactive decay accounted for 35 – 50% of the decreasing rate of total

24 ground radioactivity; the exception was Shirakawa, where radioactive decay accounted for 55

25 – 80% of the decrease. In other words, 50 – 65% of the ground radioactivity decrease was

26 likely due to land surface processes, decontamination, and re-suspension to air. As discussed

27 in Sect. 4.3, the estimated decreasing rate due to re-suspension was 2.7×10^{-7} – 8.2×10^{-6} /d,

28 which is two to three orders of magnitude smaller than the decreasing rates due to the other

29 processes (10^{-4} – 10^{-3} /d).

30 It is difficult to distinguish the contributions of land surface processes and decontamination.

31 By subtracting the radioactive decay rate (3.0 – 4.2×10^{-4} /d) and the decreasing rate due to re-

32 suspension (2.7×10^{-7} – 8.2×10^{-6} /d) from the gross decreasing rate (5.2 – 12.1 ×10^{-4} /d), the

estimated decreasing rates due to land surface processes and decontamination ranged from 1.0 – 7.9×10^{-4} /d. Matsuda et al. (2015) summarized the depth profiles of radiocesium in soil at more than 80 locations in Fukushima, including Hamadori, Abukuma, and Nakadori. They found that the radiocesium levels have been slowly migrating downward with rates ranging from 1.7 – 9.6 kg/m^2/y (equivalent to 1.1 – 6.0 mm/y for a dust particle density of 2650 kg/m^3 and a porosity of 0.4 m^3/m^3, for example). Evrard et al. (2015) summarized that significant transfer of particulate-bound radiocesium occurs during major rainfall and runoff events (e.g. typhoons and spring snowmelt). Together with the relaxation depth – dose rate relationship provided by Saito and Petoussi-Hess (2014), the decreasing rate due to land surface processes such as downward migration, runoff, and erosion could be quantified and thus the decontamination effect could be separately extracted.

5.4 Future issues

Issues that remain to be resolved in future research are summarized in the section. First of all, re-suspension from biota could be predominant in the warm season but the re-suspension sources as well as mechanisms remain essentially unknown. Further study is needed to understand the mechanism based on field experiments and numerical simulations. The current estimation could account for the measured background concentration (0.1 – 1 mBq/m^3) but could not reproduce the observed sporadic peak concentration (1 – 10 mBq/m^3) at the Namie site. Further study is needed to identify the cause. The dust flux module has been validated at a single location. The module needs to be improved to be applicable to various land use and soil texture conditions. The decontamination may reduce resuspension afterward, whereas the resuspension may occur during decontamination-related work. This effect should be evaluated in the future. The current estimation was based on a single model simulation. Variability in multi-model simulations is rather large (SCJ, 2014; Draxler et al., 2015) and therefore multi-model assessment will be indispensable for long-term re-suspension analysis.

6 Conclusions

The long-term effect of ^{137}Cs re-suspension from contaminated soil and biota due to the Fukushima nuclear accident has been quantitatively assessed using a numerical simulation, a field experiment on dust emission in the contaminated area (Namie, Fukushima), and air concentration measurements inside (Namie) and outside (Tsukuba, Ibaraki) of the area. The

1 re-suspension mechanism remains unknown. We therefore utilized the observational data

2 obtained both inside and outside the contaminated area, together with a transport model, to

3 provide a robust budget analysis of the re-suspension, transport, and re-deposition of ^{137}Cs in

4 the eastern part (the Tohoku and Kanto regions) of Japan. Our findings are summarized as

5 follows:

6 1. Optimization of the deposition parameters of the LM for simulating the emergency

7   situation of March 2011, using aircraft observation data (NRA, 2012) and the prescribed

8   emission inventory (Katata et al., 2015), provided 0.1 (0.05 – 0.1) cm/s for a dry

9   deposition velocity over land and 0.04 (0.03 – 0.05) for a hydrometeor collection

10   efficiency for aerosols. The optimized (or validated) ranges of the deposition parameters

11   were applied to long-term re-suspension assessment for the year 2013.

12 2. Using the dust emission module (Ishizuka et al., 2016), which was developed based on

13   physical parameters, simulated ^{137}Cs re-suspension from soil multiplied by five accounted

14   for the observed ^{137}Cs surface air concentration measured at Namie during only the cold

15   season; the module underestimated the ^{137}Cs concentration by one to two orders of

16   magnitude in the warm season.

17 3. Introducing re-suspension from forest using a constant re-suspension coefficient of 10^{-7} /h

18   and monthly green area fraction could quantitatively account for the observed

19   concentration together with its seasonal variation.

20 4. The contribution from additional emission from the reactor buildings of FDNPP (10^{6}

21   Bq/h) was negligible throughout the year and underestimated the observed air

22   concentration by two to three orders of magnitude at both observation sites.

23 5. At Namie and Tsukuba, the simulated contribution of re-suspension from soil was high

24   (0.7 – 0.9) in the cold season and low (0.2 – 0.4) in the warm season; the remaining

25   contribution was from forest and was low in winter and high in summer. The contribution

26   of the re-suspension from the source area (where the aircraft-observed deposition

27   exceeded 300 kBq/m^{2}) to the air concentration at Namie was 0.8 – 0.9 throughout the

28   year, while that at Tsukuba varied from 0.1 to 0.4, and was high in the summer and low

29   in the winter.

30 6. The simulated total re-suspended amount for the whole region was 1.28 TBq, equivalent

31   to 0.048% of the aircraft-observed total deposited amount of 2.68 PBq. The total re-

deposition was 0.18 – 0.23 TBq, equivalent to 14.1 – 18.0% of the total re-suspended amount: the rest of the ^{137}Cs was transported out of the model domain. The spatial distribution of the decreasing rate of land surface ^{137}Cs due to re-suspension ranged from $2.7 \times 10^{-7} – 8.2 \times 10^{-6}$ /d.

7. The first order decrease rate of the ambient gamma dose rate in Fukushima prefecture ranged from $5.2 – 12.1 \times 10^{-4}$ /d. By subtracting the radioactive decay rate of $3.0 – 4.2 \times 10^{-4}$ /d, the ground radioactivity decay due to land surface processes, decontamination, and re-suspension was found to range from $1.0 – 7.9 \times 10^{-4}$ /d. The estimated re-suspension rate was two to three orders of magnitude lower than the decrease in rate due to the other processes, showing that re-suspension contributed negligibly towards reducing ground radioactivity.

Appendix A: Model description

The current study employs a Lagrangian type model for the simulation of emission (either point sources or areal sources), horizontal and vertical diffusion and advection, gravitational settling, dry and wet depositions, and radioactive decay in the air. As described in Sect. 2.1, the current Lagrangian Model (LM) uses simple parameterizations for dry and wet deposition schemes for computational efficiency, so long-term assessment and parameter sweep experiments are easily feasible. The source code for the model is open with the BSD 3-Clause License and is available on the web (https://ebcrpa.jamstec.go.jp/isetr_a01-1/, in Japanese, last access: 26 July 2016).

The coordinate system of the model is horizontal for longitude and latitude and vertical for pressure level, consistent with meteorological analysis data commonly used. The model can be driven only by fundamental meteorological parameters such as temperature, humidity, 3D wind field, geopotential height, and surface precipitation provided by meteorological analysis data such as GPV-MSM. The model does not need to drive meteorological models to predict detailed meteorological variables such as cloud microphysics, turbulence quantities, and surface variables. Since the temporal and spatial resolution of the meteorological analysis is not very high (e.g., 3 h and ~11 km for GPV-MSM, respectively), linear interpolation is conducted in time and space. Alternatively, higher temporal and spatial resolution can be achieved by using a meteorological model. Furthermore, although currently not implemented,

1 detailed variables predicted by a meteorological model can be used for more accurate

2 predictions of turbulent diffusion, surface flux, and dry and wet deposition.

3 In the LM model, LPs are released constantly in time but the initial activity of LPs (Bq/LP)

4 differs accordingly to the emission flux (Bq/h). The initial positions of LPs were randomly

5 distributed within a fixed volume (or line) of plume centered at a point emission source such

6 as FDNPP for the primary emission case simulation, or randomly distributed within a

7 horizontal model grid for the areal emission cases (such as re-suspension from soil and forest).

8 LPs do not disappear unless transported across lateral and upper boundaries or if they reach

9 the surface layer due to gravitational settling (technically, gravitational settling velocity in the

10 surface layer is included in the dry deposition velocity). The other processes, such as dry

11 deposition, wet deposition and radioactive decay, do not decrease the number of LPs but do

12 decrease the radioactivity carried by LPs because LPs represent an air mass rather than an

13 actual particle, except in the case of gravitational settling. The lowest level permitted for the

14 position of LPs is set as 2 m AGL and LPs going down across the level due to vertical

15 turbulent motion will rebound at the level and go up. An LP whose radioactivity is smaller

16 than a preset value, i.e., 10^{-10} Bq, due to deposition or radioactive decay will disappear from

17 the computation to maintain computational efficiency, since the cost of the computation is

18 proportional to the number of LPs in the model domain. To output the model results, the LP

19 fields are converted to Eulerian concentration (Bq/m^3) and deposition (Bq/m^2) fields on a

20 prescribed coordinate system of grids. In Lagrangian type models, the spatial resolution of

21 tracer emission, concentration, and deposition fields can be set independent of each other and

22 with the spatial resolution of meteorological fields. In the current implementation of the LM,

23 the coordinate system of meteorological fields and radioactivity fields is horizontal for

24 common (longitude and latitude) but vertical for different (pressure level and meters AGL,

25 respectively).

26 The horizontal and vertical diffusion calculation followed JMA (2008), using the horizontal

27 diffusion scheme of Uliasz (1990) with a constant horizontal diffusivity of 5.864×10^4 m^2/s

28 and using a vertical diffusivity calculated based on Louis et al. (1982) (see Eqs. 8.1.8 through

29 8.1.15 of JMA (2008) for details). The incremental change in location of an LP δx (y, z) after

30 a time step δt was defined as

31 $$\delta x = \frac{\mathrm{d}x}{\mathrm{d}t} G \delta t \, , \tag{A1}$$

1 where G is the normalized Gaussian random number (average = 0, standard deviation = 1). δt

2 is set large enough for computational efficiency but without violating the Courant-Friedrichs-

3 Lewy (CFL) condition of $\delta t < 0.5\ U/\Delta x$, where U (or dx/dt) is the typical wind speed and Δx is

4 the grid size in the direction of U. However, the selection of δt is not critical because every

5 time step prior to applying Eq. (A1) time splitting is made so that the split step always

6 satisfies the CFL condition.

7 The wet scavenging rate Λ_{wet} (/s) is simply parameterized as a function of the surface

8 precipitation rate P (mm/s) as

9 $$\Lambda_{wet} = \frac{3}{4}\frac{E_c(a_m, r_m)}{a_m}P\,, \tag{A2}$$

10 where E_c is the collection efficiency of aerosols by the hydrometeor, and a_m and r_m are the

11 mean radii of the hydrometeor and aerosols, respectively (JMA, 2008). Empirically, a_m is

12 characterized by P as

13 $$a_m = 0.35 P^{0.25}\,. \tag{A3}$$

14 JMA (2008) uses 0.05 for E_c. In the current study, instead of explicitly predicting E_c, its range

15 was set for the sensitivity tests as listed in Table 2.

16 Conceptually, Eq. (A2) is the formulation for the washout process, i.e., the collection of

17 aerosols by the settling hydrometeor particles such as rain and snow. a_m and E_c should differ

18 for rain and snow, but common parameters are used in the current simulation. Also, Eq. (A2)

19 is not applicable for the rainout process, since this process—cloud condensation nuclei or ice

20 nuclei activation and deposition via subsequent cloud microphysical processes— is totally

21 different from the washout process. Because meteorological models were not utilized in this

22 study and thus only relative humidity and surface precipitation rate are available and no cloud

23 microphysical information (such as hydrometeors mixing ratio in each model grid) is

24 available, Eq. (A2) is applied for all the LPs located above the grid with P. In order to partly

25 account for the rainout process, Eq. (A2) is not applied to LPs in a grid, where the relative

26 humidity is lower than the minimum value, set as 95% in the simulation.

27 The dry deposition velocity v_d (m/s) of aerosols (or gases) is conventionally formulated, using

28 an electrical analogy, as an inverse of the summation of resistances (s/m) representing

29 turbulent diffusion in the surface layer, Brownian diffusion (or molecular diffusion for gases),

30 interaction with the land surface (soil, water and vegetation), and gravitational settling for

1 aerosols (e.g., Wesely and Hicks, 2000). Therefore, v_d is a function of height as well as of

2 turbulent flux and surface conditions. Nevertheless, v_d is set as constant in the simulation, but

3 the height dependency of v_d is considered in the dry scavenging rate Λ_{dry} (/s), following

4 Furuno et al. (1999) as

5 $$\Lambda_{dry} = \frac{2}{z_{srf}} \left(1 - \frac{z}{z_{srf}} \right) v_d, \qquad (A4)$$

6 where z is the height of the LP (m AGL) and z_{srf} is the surface layer height set as 100 m AGL

7 in the study. Instead of explicitly predicting v_d, its range was set at around 0.1 cm/s, a typical

8 speed for a range of aerosols around 1 μm in diameter, for the sensitivity tests, as listed in

9 Table 2. The value of v_d is applied over land, whereas v_d over the ocean is multiplied by 0.1,

10 because v_d over a flat surface is approximately one and two orders of magnitude smaller than

11 v_d over short vegetation such as grass and tall vegetation such as forest, respectively (e.g.,

12 Petroff and Zhang, 2010).

14 **Appendix B: Statistical accuracy of the current simulation setting**

15 Because the statistical error of Lagrangian simulation is inversely proportional to the square

16 of the number of LPs, the statistical accuracy of the current simulation setting was evaluated

17 using the following measures (relative errors of quantities of the sensitivity runs to those of

18 the reference run):

19 $$E_{con}(x,y) = \frac{\left| C_{sens}(x,y) - C_{ref}(x,y) \right|}{C_{ref}(x,y)}, \qquad (B1)$$

20 $$E_{dep}(x,y) = \frac{\left| D_{sens}(x,y) - D_{ref}(x,y) \right|}{D_{ref}(x,y)}, \qquad (B2)$$

21 where x and y indicate grid points on the longitudinal and latitudinal axes, respectively. C_{sens}

22 and D_{sens} indicate temporal mean surface concentrations (Bq/m^3) and temporal cumulative

23 depositions (Bq/m^2) of the sensitivity runs, respectively. C_{ref} and D_{ref} are the same as C_{sens}

24 and D_{sens} but for the reference run. E_{con} and E_{dep} were sampled only at grids where $C_{ref}(x,y)$

25 and $D_{ref}(x,y)$ are greater than their areal mean values, respectively.

B.1 Point source case

The number emission rate of LPs, N_{LP}, was set as 32,000 /h (=N_{LP_ref}) for a point source emission case such as the primary emission in March 2011 and additional emission from the reactor buildings in 2013. The median values together with the 25th and 75th percentile values of E_{con} and E_{dep} of the sensitivity runs (sensitivity to deposition parameters and sensitivity to N_{LP}) against the reference run are listed on the top half rows of Table B1. Both E_{con} and E_{dep} of $N_{LP\_ref} \times 4$ were significantly lower than those for the deposition parameters sensitivity run. This result indicates that 32,000 /h for N_{LP} was sufficient to allow a statistically significant simulation for the purpose of this study, as shown in Figs. 4 and 5: the difference in concentration and deposition due to the deposition parameters was much larger than the difference due to model uncertainty in N_{LP}. E_{con} and E_{dep} of $N_{LP\_ref} \times 0.25$ (which are also smaller than those of the deposition parameters sensitivity run) are larger than those of $N_{LP\_ref} \times 4$, indicating fairly well accuracy convergence of the LM model.

B.2 Areal emission case

N_{LP_ref} was 16 /h/grid for the areal emission case simulating re-suspension from soil and forests in 2013. The lower half of Table B1 is the same as the upper half except for the areal emission case (re-suspension from forest). Both E_{con} and E_{dep} of $N_{LP\_ref} \times 4$ were much lower than those for the deposition parameters sensitivity run, indicating that 16 /h/grid supports a statistically significant simulation for the purpose of this study, as shown in Figs. 7 - 12. Usually, Eulerian-type models are appropriate for solving areal emission problems—Lagrangian-type models require many more LPs for areal emission cases compared to point source cases and thus become computationally too expensive. In the case of this simulation, especially for the concentration, sensitivity to deposition parameters was much more significant than sensitivity to model uncertainty in N_{LP} using the sufficiently small number of $N_{LP\_ref} = 16$ /h/grid. E_{con} and E_{dep} of $N_{LP\_ref} \times 4$ are smaller than those of $N_{LP\_ref} \times 0.25$, indicating fairly accuracy convergence of the LM model.

Acknowledgements

This research was mainly supported by Grants-in-Aid for Scientific Research on Innovative Areas (24110002 and 20110003) from the Ministry of Education, Culture, Sports, Science and Technology (MEXT), and partly supported by the Japan Society for the Promotion of

Science (JSPS), Ministère des Affaires Étrangères et du Développement International (MAEDI) under the Japan-France Integrated Action Program (SAKURA), and by KAKENHI Grant Numbers 15K16121, 24340115, and 26310201 from MEXT. Partial expenses were covered by the Japanese Radioactivity Survey from the NRA, Japan. The authors are grateful for useful discussions with and comments from Prof. Yuichi Moriguchi of University of Tokyo, Prof. Hiromi Yamazawa of Nagoya University, and Dr. Haruo Tsuruta of Remote Sensing Technology Center of Japan (RESTEC). The LM was developed by MI, CY, and MK.

References

Adachi, K., Kajino, M., Zaizen, Y., and Igarashi, Y.: Emission of spherical cesium-bearing particles from an early stage of the Fukushima nuclear accident, Scientific Report, 3, 2554, doi:10.1038/srep02554, 2013.

Chino, M., Nakayama, H., Nagai, H., Terada, H., Katata, G., and Yamazawa, H.: Preliminary estimation of release amounts of ^{131}I and ^{137}Cs accidentally discharged from the Fukushima Daiichi nuclear power plant into atmosphere, J. Nucl. Sci. Technol., 48, 1129-1134, 2011.

Danielache, S. O., Yoshikawa, C., Priyadarshi, A., Takemura, T., Ueno, Y., Thiemens, M. H.,and Yoshida, N.: An estimation of the radioactive ^{35}S emitted into the atmospheric from the Fukushima Daiichi Nuclear Power Plant by using a numerical simulation global transport, Geochemical Journal, 46, 355-339, 2012.

Danielache, S. O., Yoshikawa, C., Kajino, M., Itou, S., Kakeya, W., Yoshida, N., Igarashi, Y.: Radioactive ^{35}S emitted from the Fukushima Nuclear Power Plan studied by a modified regional model, 2016, manuscript in preparation.

Draxler, R., Arnold, D., Chino, M., Galmarini, S., Hort, M., Jones, A., Leadbetter, S., Malo, A., Maurer, C., Rolph, G., Saito, K., Servranckx, R., Shimbori, T., Solazzo, E., Wotawa, G.: World Meteorological Organization's model simulations of the radionuclide dispersion and deposition from the Fukushima Daiichi nuclear power plant accident, J. Environ. Radioact., 139, 172-184, 2015.

Evangeliou, N., Balkanski, Y., Cozic, A., Møller, A. P.: Global and local cancer risks after the Fukushima Nuclear Power Plant accident as seen from Chernobyl: A modeling study for radiocaesium (^{134}Cs & ^{137}Cs)", Environ. Int., 64, 17–27, 2014. Evrard, O., Laceby, J. P., Lepage, H., Onda, Y., Cerdan, O., Ayrault, S.: Radiocesium transfer from hillslopes to the

Pacific Ocean after the Fukushima Nuclear Power Plant accident: A review, J. Environ. Radioact., 148, 92-110, 2015.

Furuno, A., Chino, M., and Yamazawa, H.: Worldwide version of System of Prediction of Environmental Emergency Dose Information (WSPEEDI) Model Code (II) – Three-dimensional Atmospheric Dispersion Model for Synoptic Scale: GEARN, JAERI-Data/Code 99-044, Japan Atomic Energy Research Institute, Japan (in Japanese), 68 pp., 1999.

Garger, E.K., Paretzke, H.G., Tschiersch, J.: Measurement of resuspended aerosol in the Chernobyl area. Part III: size distribution and dry deposition velocity of radioactive particles during anthropogenic enhanced resuspension, Radiation and Environmental Biophysics 37, 201-208, 1998.

Garger, E. K., Kuzmenko, Y. I., Sickinger, S., Tschiersch, J.: Prediction of the ^{137}Cs activity concentration in the atmospheric surface layer of the Chernobyl exclusion zone, J. Environ. Radioact., 110, 53-8, 2012.

Girard, S., Mallet, V., Korsakissok, I., and Mathieu, A.: Emulation and Sobl' sensitivity analysis of an atmospheric dispersion model applied to the Fukushima nuclear accident, J. Geophys. Res., 2016, in press.

Groëll J., Quélo, D., and Mathieu, A.: Sensitivity analysis of the modelled deposition of ^{137}Cs on the Japanese land following the Fukushima accident, Int. J. of Environment and Pollution, 55, 67-75, 2014.

Gutman, G., and Ignatov, A.: The derivation of green vegetation fraction from NOAA/AVHRR data for use in numerical weather prediction models, Int. J. Remote Sens., 19, 1533-1543, 1998.

Hatano, Y., and Hatano N.: Formula for the resuspension factor and estimation of the date of surface contamination, Atmos. Environ., 37, 3475-3480, 2003.

Hirao, S., Yamazawa, H., Nagae, T.: Estimation of release rate of iodine-131 and cesium-137 from the Fukushima Daiichi nuclear power plant, J. Nucl. Sci. Technol., 50, 139-147, doi:10.1080/00223131.2013.757454, 2013.

Holländer, W., Garger, E.: Contamination of Surface by Resuspended Material. ECP–1, Final Report, Rep. EUR 16527. Office for Official Publications of the European Communities, Luxembourg, 1996.

Hososhima, M. and Kaneyasu, N.: Altitude-dependent distribution of ambient gamma dose rates in mountainous area of Japan caused by the Fukushima nuclear accident. Environ. Sci. Technolo., 49(6), 3341-3348, 2015.

Igarashi, Y., Kajino, M., Zaizen, Y., Adachi, K., and Mikami, M.: Atmospheric radioactivity over Tsukuba, Japan: a summary of three years of observations after the FDNPP accident, Progress in Earth and Planetary Science, 2:44, doi:10.1186/s40645-015-0066-1, 2015.

Ishizuka, M, Mikami, M., Tanaka, T. Y., Igarashi, Y., Kita, K., Yamada, Y., Yoshida, N., Toyoda, S., Satou, Y., Kinase, T., Ninomiya, K., Shinohara, A.: Use of a size-resolved 1-D resuspension scheme to evaluation resuspended radioactive material associated with mineral dust particles from the ground surface, J. Environ. Radioact., 13pp., doi:10.1016/j.jenvrad.2015.12.023, 2016, in press.

JMA: Japan Meteorological Agency's Non-Hydrostatic Model II, *Suuchi Yohoka Hokoku Bessatsu* (Additional Volume to Report of Numerical Prediction Division) 54, 265 pp., 2008 (in Japanese).

Kaneyasu, N., Ohashi, H., Suzuki, F., Okada, T., and Ikemori, F.: Sulfate aerosol as a potential transport medium of radiocesium from the Fukushima nuclear accident, Environ. Sci. Technol. 46, 5720-5726, 2012.

Katata, G., Terada, H., Nagai, H., and Chino, M.: Numerical reconstruction of high dose rate zones due to the Fukushima Daiichi Nuclear Power Plant accident, J. Environ. Radioact., 111, 2-12, 2012a.

Katata, G., Ota, M., Terada, H., Chino, M., and Nagai, H.: Atmospheric discharge and dispersion of radionuclides during the Fukushima Dai-ichi Nuclear Power Plant accident, Part I: Source term estimation and local-scale atmospheric dispersion in early phase of the accident, J. Environ. Radioact, 109, 103-113, doi:10.1016/j.jenvrad.2012.02.006, 2012b.

Katata, G., Chino, M., Kobayashi, T., Terada, H., Ota, M., Nagai, H., Kajino, M., Draxler, R., Hort, M. C., Malo, A., Torii, T., and Sanada, Y.: Detailed source term estimation of the atmospheric release for the Fukushima Daiichi Nuclear Power Station accident by coupling simulations of an atmospheric dispersion model with an improved deposition scheme and oceanic dispersion model. Atmos. Chem. Phys., 15, 1029-1070, 2015.

Kinase, T., Kita, K. Igarashi, Y., Adachi, K., Ninomiya, K., Shinohara, A., Okochi, H., Ogata, Y., Ishizuka, M., Toyoda, S., Yamada, K., Yoshida, N., Zaizen, Y., Mikami, M., Demizu, H.,

and Onda, Y.: Seasonal variation in activity concentration of atmospheric [134,137]Cs and their possibile resuspension host aerosol observed at Tsuahima and Yamakiya, Fukushima, 2016, in preparation.

Kristiansen, N. I., Stohl, A., Olivie, D. J. L., Croft, B., Sovde, O. A., Klein, H., Christoudias, T., Kunkel, D., Leadbetter, S. J., Lee, Y. H., Zhang, K., Tsigaridis, K., Bergman, T., Evangeliou, N., Wang, H., Ma, P.-L., Easter, R. C., Rasch, P. J., Liu, X., Pitari, G., Di Genova, G., Zhao, S. Y., Balkanski, Y., Bauer, S. E., Faluvegi, G. S., Kokkola, H., Martin, R. V., Pierce, J. R., Schulz, M., Shindell, D., Tost, H., and Zhang, H.: Evaluation of observed and modelled aerosol lifetimes using radioactive tracers of opportunity and an ensemble of 19 global models, Atmos. Chem. Phys., 16, 3525-3561, doi:10.5194/acp-16-3525-2016, 2016.

Loosmore, G. A., Hunt, J. R.: Dust resuspension without saltation, J. Geophys. Res., 105(D16), 20,663-20,671, doi:10.1029/2000JD900271, 2002.

Louis, J. F., Tiedtke, M., Geleyn, J. F.: A short history of the PBL parameterization at ECMWF, *Workshop on planetary boundary layer parameterization. ECMWF*, 59-80, 1982.

MAFF (Ministry of Agriculture, Forestry and Fisheries), Fukushima Prefecture, Tohoku Agricultural Research Center, National Institute for Agro-Environmental Sciences: Investigation of the cause for brown rice exceeding the allowable radiocesium concentration, available at http://www.maff.go.jp/j/kanbo/joho/saigai/fukusima/pdf/150526_youin_chosa.pdf (last access, 26 July 2016), 2015 (in Japanese).

Masson, O., Baeza, A., Bieringer, J., Brudecki., Bucci, S., Cappai, M., Carvalho, F. P., Connan, O., Cosma, C., Dalheimer, A., Didier, D., Depuydt, G., De Geer, L. E., De Vismes, A., Gini, L., Groppi, F., Gudnason, K., Gurriaran, R., Hainz, D., Halldórsson, O., Hammond, D., Hanley, O., Holey, K., Homoki, Zs., Ioannidou, A., Isajenko, K., Jankovic, M., Katzlberger, C., Kettunen, M., Kierepko, R., Kontro, R., Kwakman, P. J. M., Lecomte, M., Leon Vintro, L., Leppänen, A.-P., Lind, B., Lujaniene, G., Mc Ginnity, P., Mc Mahon, C., Malá, H., Manenti, S., Manolopoulou, M., Mattila., A., Mauring., A., Mietelski, J. W., Moller, B., Nielsen, S. P., Nikolic, J., Overwater, R. M. W., Pálsson, S. E., Papastefanou, C., Penev, I., Pham, M. K., Povinec, P. P., Ramebäck, H., Reis, M. C., Ringer, W., Rodriguez, A., Rulik, P., Saey, P. R. J., Samsonov, V., Schlosser, C., Sgorbati, G., Silobritiene, B. V., Söderström, C., Sogni, R., Solier, L., Sonck, M., Steinhauser, G., Steinkopff, T., Steinmann, P., Stoulos, S., Sýkora, I., Todorovic, D., Tooloutalaie, N., Tositti, L., Tschiersch, J., Ugron, A., Vagena, E., Vargas, A., Wershofen, H., Zhukova, O. Tracking of Airborne Radionuclides from the

Damaged Fukushima Dai-Ichi Nuclear Reactors by European Networks. Environ. Sci. Technol. 2011, 45 (18), 7670-7677, 2011.

Masson, O., Ringer, W., Malá, H., Rulik, P., Dlugosz-Lisiecka, M., Eleftheriadis, K., Meisenberg, O., De Vismes-Ott, A., and Gensdarmes, F.: Size distribution of airborne radionuclides from the Fukushima Nuclear Accident at several places in Europe, Environ. Sci. Technol., 47, 10995-11003, 2013.

Matsunami H., Murakami, T., Fujiwara, H., and Shinano, T.: Evaluation of the cause of unexplained radiocaesium contamination of brown rice in Fukushima in 2013 using autoradiography and gamma-ray spectrometry, Scientific Report, 6, 20386, doi:10.1038/srep20386, 2016.

METI (Ministry of Economy, Trade and Industry): Convention on Nuclear Safety National Report of Japan for the Second Extraordinary Meeting, July 2012, Government of Japan, available at www.meti.go.jp/english/press/2012/pdf/0705_01b.pdf (last access: 26 July 2016), 2012.

Miller, D. A. and White, R. A.: A conterminous United States multi-layer soil characteristics data set for regional climate and hydrology modeling, Earth Interactions, 2, 1-26, 1998.

Matsuda, N., Mikami, S., Shimoura, S., Takahashi, J., Nakano, M., Shimada, K., Uno, K., Hagiwara, S., and Saito, K.: Depth profiles of radioactive cesium in soil using a scraper plate over a wide area surrounding the Fukushima Dai-ichi Nuclear Power Plant, Japan., 139, J. Environ. Radioact., 427-434, 2015.

Morino, Y., Ohara, T., and Nishizawa, M.: Atmospheric behavior, deposition, and budget of radioactive materials from the Fukushima Daiichi nuclear power plant in March 2011, Geophys. Res. Lett. 38, doi:10.1029/2011GL048689, 2011.

Morino, Y., Ohara, T., Watanabe, S., Hayashi, S., and Nishizawa, M.: Episode analysis of deposition of radiocesium from the Fukushima Daiichi Nuclear Power Plant accident, Environ. Sci. Technol., 47, 2314-2322, 2013.

NRA (Nuclear Regulation Authority): Airborne Monitoring Results in each prefecture, available at: http://radioactivity.nsr.go.jp/en/list/203/list-1.html (last access: 26 July 2016), 2012.

NRA: Assessment of radionuclide emission involved in the debris removal operations for reactor 3; Handout for the 28th meeting on the supervision of a specific nuclear facility, available at http://www.nsr.go.jp/data/000051154.pdf (last access, 26 July 2016), 2014 (in Japanese).

Ohmori, Y., Kajikawa, M., Nishida, S., Tanaka, N., Kobayashi, N. I., Tanoi, K., Furukawa, and J., Fujiwara, T.: The effect of fertilization on cesium concentration of rice grown in a paddy field in Fukushima Prefecture in 2011 and 2012, J. Plant Res., 127, 1, 67-71, 2014.

Oura, Y., Ebihara, M., Tsuruta, H., Nakajima, T., Ohara, T., Ishimoto, M., Sawahata, H., Katsumura, Y., and Nitta, W.: A database of hourly atmospheric concentrations of radiocesium (^{134}Cs and ^{137}Cs) in suspended particulate matter collected in March 2011 at 99 air pollution monitoring stations in Eastern Japan, Journal of Nuclear and Radiochemical Sciences, 15(2), 15-26, 2015.

Petroff, A. and Zhang L.: Development and validation of a size-resolved particle dry deposition scheme for application in aerosol transport models, Geosci. Model Dev. 3, 753-769, 2010.

Pöhlker C., Wiedemann, K. T., Sinha, B., Shiraiwa, M., Gunthe, S. S., Smith, M., Su, H., Artaxo, P., Chen, Q., Cheng, Y., Elbert, W., Gilles, M. K., Kilcoyne, A. L. D., Moffet, R. C>, Weigand, M., Matin, S. T., Pöschl, U., and Andreae, M. O.: Biogenic potassium salt particles as seeds for secondary organic aerosol in the Amazon, Science, 337, 1075-1078, 2012.

Quérel, A., Roustan, Y., Quélo, D., and Benoit, J. -P.: Hints to discriminate the choice of wet deposition models applied to an accidental radioactive release, Int. J. of Environment and Pollution, in review.

Saito, K., Petoussi-Henss, N.: Ambient dose equivalent conversion coefficients for radionuclides exponentially distributed in the ground, J. Nucl. Sci. Techonol., 51(10), 1274-1287, doi:10.1080/00223131.2014.919885, 2014.

Saito, K., Shimbori, T., and Draxler, R.: JMA's regional atmospheric transport model calculations for the WMO technical task team on meteorological analyses for Fukushima Daiichi Nuclear Power Plant accident, J. Environ. Raioact., 139, 185-199, 2015.

Saunier, O., Mathieu, A., Didier, D., Tombette, M., Quelo, D., Winiarek, V., and Bocquet, M.: An inverse modeling method to assess the source term of the Fukushima Nuclear Power

Plant accident using gamma dose rate observations, Atmos. Chem. Phys., 13, 11403-11421, doi:10.5194/acp-13-11403-2013, 2013.

SCJ (Science Council of Japan): A review of the model comparison of transportation and deposition of radioactive materials released to the environment as a result of the Tokyo Electric Power Company's Fukushima Daiichi Nuclear Power Plant accident, available at http://www.scj.go.jp/ja/info/kohyo/pdf/kohyo-22-h140902-e1.pdf (last access: 26 July 2016), 2014.

Sekiyama, T. T., Kunii, M., Kajino, M., and Shimbori, T.: Horizontal resolution dependence of atmospheric simulations of the Fukushima nuclear accident using 15-km, 3-km, and 500-m grid models, J. Meteor. Soc. Japan, 93, 49-64, 2015.

Sekiyama, T. T., Kajino, M., and Kunii, M.: Ensemble dispersion simulation of a point-source radioactive aerosol using a square root Kalman filter, J. Geophys. Res., 2016, in review.

Skamarock, W. C., Klemp, J. B., Dudhia, J., Grill, D. O., Barker, D. M., Duda, M. G., Huang, X. Y., Wang, W., and Powers, J. G.: A description of the advanced research WRF version 3, Tech. Note, NCAR/TN~475+STR, 125 pp., Natl. Cent. For Atmos. Res., Boulder, Colo., 2008.

Steinhauser, G., Niisoe, T., Harada, K. H., Shozugawa, K., Schneider, S., Synal, H.-A, Walther, C., Christl, M., Nanba, K., Ishikawa, H., and Koizumi, A: Post-accident sporadic releases of airborne radionuclides from the Fukushima Daiichi Nuclear Power Plant Site, Environ. Sci. Technol., 49, 14028-14035, doi:10.1021/acs.est.5b03155, 2015.

Stohl, A. Seibert, P., Wotawa, G., Arnold, D., Burkhart, J. F., Eckhardt, S., Tapia, C., Vargas, A., and Yasunari, T. J.: Xenon-133 and caesium-137 releases into the atmosphere from the Fukushima Dai-ichi nuclear power plant: determination of the source term, atmospheric dispersion, and deposition. Atmos. Chem. Phys., 12, 2313-2343, 2012.

TEPCO (Tokyo Electric Power Co., Inc.): Estimation of additional emissions from nuclear reactor buildings (30 July 2012), available at: http://www.tepco.co.jp/nu/fukushima-np/roadmap/images/m120730_05-j.pdf (last access: 26 July 2016), 2012 (in Japanese).

TEPCO: Estimation of the additional emission from nuclear reactor buildings (30 May 2013), available at: http://www.tepco.co.jp/nu/fukushima-np/roadmap/images/d130530_05-j.pdf (last access: 26 July 2016), 2013 (in Japanese).

TEPCO: Estimation of the additional emission from nuclear reactor buildings (27 March 2014), available at: http://www.tepco.co.jp/nu/fukushima-np/roadmap/images/d140327_06-j.pdf (last access: 26 July 2016), 2014a (in Japanese).

TEPCO: Estimation of the additional emission from nuclear reactor buildings (25 December 2014), available at: http://www.tepco.co.jp/nu/fukushima-np/roadmap/images/d141225_08-j.pdf (last access: 26 July 2016), 2014b (in Japanese).

TEPCO: Estimation of radioactive material released during debris removal operations at reactor unit 3 of the Fukushima Daiichi Nuclear Power Plant in August 2013, available at http://www.nsr.go.jp/data/000051136.pdf (last access: 26 July 2016), 2014c (in Japanese).

TEPCO: Estimation of the additional emission from nuclear reactor buildings (9 October 2015), available at: http://www.tepco.co.jp/life/custom/faq/images/d151109_11-j.pdf (last access: 26 July 2016), 2015 (in Japanese).

Terada, H., Katata, G., Chino, M., and Nagai, H.: Atmospheric discharge and dispersion of radionuclides during the Fukushima Dai-ichi Nuclear Power Plant accident, Part II: Verification of the source term and analysis of regional-scale atmospheric dispersion, J. Environ. Radioact., 112, 141-154, 2012.

Tsuruta, H., Oura, Y., Ebihara, M., Ohara, T., and Nakajima, T.: First retrieval of hourly atmospheric radionuclides just after the Fukushima accident by analysing filter-tapes of operational air pollution monitoring stations, Scientific Reports, 4, 6717, doi:10.1038/srep06717, 2014.

Uliasz, M.: Development of the mesoscale dispersion modelling system using personal computers. Part I: Models and computer implementation. Z. Meteor., 40, 110-120, 1990.

Wesely, M. L. and Hicks, B. B.: A review of the current status of knowledge on dry deposition, Atmos. Environ., 34, 2261-2282, 2000.

Winiarek, V., Bocquet, M., Saunier, O., and Mathieu, A.: Estimation of errors in the inverse modeling of accidental release of atmospheric pollutant: Application to the reconstruction of the cesium-137 and iodine-131 source terms from the Fukushima Daiichi power plant, J. Geophys. Res., 117, D05122, 16 pp, doi:10.1029/2011JD016932, 2012.

Winiarek, V., Bocquet, M., Duhanyan, N., Roustan, Y., Saunier, O., and Mathieu, A.: Estimation of the caesium-137 source term from the Fukushima Daiichi nuclear power plant

1 using a consistent joint assimilation of air concentration and deposition observations, Atmos.
2 Environ., 82, 268-279, 2014.

3 Yasunari, T. J., Stohl A., Hayano R. S., Burkhart J. F., Eckhardt S., and Yasunari T.: Cesium-
4 137 deposition and contamination of Japanese soils due to the Fukushima nuclear accident.
5 Proc. Natl. Acad. Sci., 108, 19530-19534, 2011.

6 Yumimoto, K., Mirno, Y., Ohara, T., Oura, Y., Ebihara, M., Tsuruta, H., and Nakajima, T.:
7 Inverse modeling of the 137Cs source term of the Fukushima Dai-ichi Nuclear Power Plant
8 accident constrained by a deposition map monitored by aircraft, J. Environ. Radioact., 2016,
9 in review.

1   Table 1. The observation sites and monitoring posts used to provide data for this study.

Name	Location	Description
Observation sites		
Namie (Tsushima)	140.7683 °E, 37.5621 °N	Namie High School, Tsushima Campus[1]
Tsukuba	140.1254 °E, 36.0551 °N	Meteorological Research Institute
Monitoring posts		
Okuma	140.9969 °E, 37.4163 °N	Ottozawa 3 Community Center[2]
Namie (Omaru)	140.9296 °E, 37.4665 °N	Omaru Multipurpose Community Center[3]
Iitate	140.7385 °E, 37.6772 °N	Iitate Junior High School[4]
Kawamata	140.6979 °E, 37.5836 °N	Yamakiya Otsu 8 Community Firehouse[5]
Fukushima	140.4765 °E, 37.6870 °N	Fukushima-Minami Fire Department
Shirakawa	140.1904 °E, 37.1241 °N	Takayama-Kita Park

2   1.   Original location (now moved to Nihonmatsu city).

3   2.   Ottozawa San-ku Chiku Shukaijo (in Japanese)

4   3.   Omaru Tamokuteki Shukaijo (in Japanese)

5   4.   Original location (now moved to Fukushima city).

6   5.   Yamakiya Otsu Hachi-ku Community Shoubou Center (in Japanese)

Table 2. ^{137}Cs budget and statistical analysis for the comparison of observed and simulated deposition data for March 2011.

	E_c[a]	v_d[b]	D_{all}[c]	D_{land}[d]	FB[e]	R[f]	$FA2$[g]	$FA5$[h]
	(-)	(cm/s)	(PBq)	(PBq)	(-)	(-)	(-)	(-)
Sensitivity test								
Range	0.02 – 0.06	0.05 – 0.15	3.4 – 4.7	2.0 – 2.8	-0.25 – 0.00050	0.73 – 0.78	0.25 – 0.30	0.63 – 0.77
Optimization used for the re-suspension analysis for 2013								
Reference	0.04	0.10	4.2	2.5	-0.062	0.75	0.28	0.74
Optimized range	0.03 – 0.05	0.05 – 0.10	3.7 – 4.3	2.2 – 2.6	-0.18 – -0.036	0.74 – 0.77	0.26 – 0.30	0.68 – 0.74
Reference values								
Observed deposition over land D_{obs} (NRA, 2012)			2.68 PBq					
Emission amount (Katata et al., 2015)			14.1 PBq					

[a] Collection efficiency, see Eq. (A2) [b] Dry deposition velocity over land, see Eq. (A4). [c] Simulated deposited amount over the whole model domain. [d] Simulated deposited amount only over land. [e] Fractional bias between D_{land} and $D_{obs.}$ [f] Correlation coefficient between each grid cell of the observed and simulated deposition (linear vs. linear). [g] Fraction of simulated values within a factor of 2 of the observed values. [h] Fraction of simulated values within a factor of 5 of the observed values. [f, g, h] Compared only at grids where the observed values are greater than 10 kBq/m^2.

1 Table 3. Statistical analysis for the comparison of observed and simulated ^{137}Cs air
2 concentration at Namie and Tsukuba for 2013.

Site	N	Median, Obs.	Median, Sim.	R	FA2	FA5	FA10
	(-)	(mBq/m^3)	(mBq/m^3)	(-)	(-)	(-)	(-)
Namie	311	0.71	0.69	0.12	0.67	0.94	0.99
Tsukuba	74	0.022	0.024	0.19	0.70	0.95	1.00

Table B1. Statistical measures of temporal mean ^{137}Cs surface concentration (E_{con}) and cumulative deposition (E_{dep}) of the sensitivity runs against the reference run for (top) the point source case and (bottom) the areal emission case.

	Number emission rate of LP, N_{LP} (/h/grid)	$E_c{}^a$ (-)	$v_d{}^b$ (cm/s)	Median (25th – 75th percentile) of $E_{con}{}^c$ (%)	Median (25th – 75th percentile) of $E_{dep}{}^d$ (%)
Point source case, March 2011					
Reference run	32,000	0.04	0.01	-	-
Sensitivity runs					
Deposition parameters	32,000	0.03 – 0.05	0.05 – 0.01	2.7 (0.37 – 5.0)	7.5 (3.6 – 13)
$N_{LP\_ref} \times 4$	128,000	0.04	0.01	0.51 (0.21 – 0.96)	0.72 (0.32 – 1.5)
$N_{LP\_ref} \times 0.25$	8,000	0.04	0.01	0.95 (0.39-1.8)	1.6 (0.73 – 2.9)
Areal emission case, 2013 (re-suspension from forest)					
Reference run	16	0.04	0.10	-	-
Sensitivity runs					
Deposition parameters	16	0.03 – 0.05	0.05 – 0.01	7.3 (2.6 – 13)	7.7 (3.6 – 17)
$N_{LP\_ref} \times 4$	64	0.04	0.10	0.39 (0.17 – 0.78)	2.0 (1.3 – 2.6)
$N_{LP\_ref} \times 0.25$	4	0.04	0.10	0.78 (0.34-1.5)	2.3 (1.5 – 3.1)

[a] Collection efficiency, see Eq. (A2). [b] Dry deposition velocity over land, see Eq. (A4). [c] Relative errors of temporal mean surface concentration at each grid cell of the sensitivity run to that of the reference run, see Eq. (B1). [d] same as E_{con} but for cumulative deposition, see Eq. (B2).

Name of prefectures: 1. Miyagi, 2. Fukushima, 3. Ibaraki, 4. Tochigi,
5. Gunma, 6. Saitama, 7. Chiba, 8. Tokyo
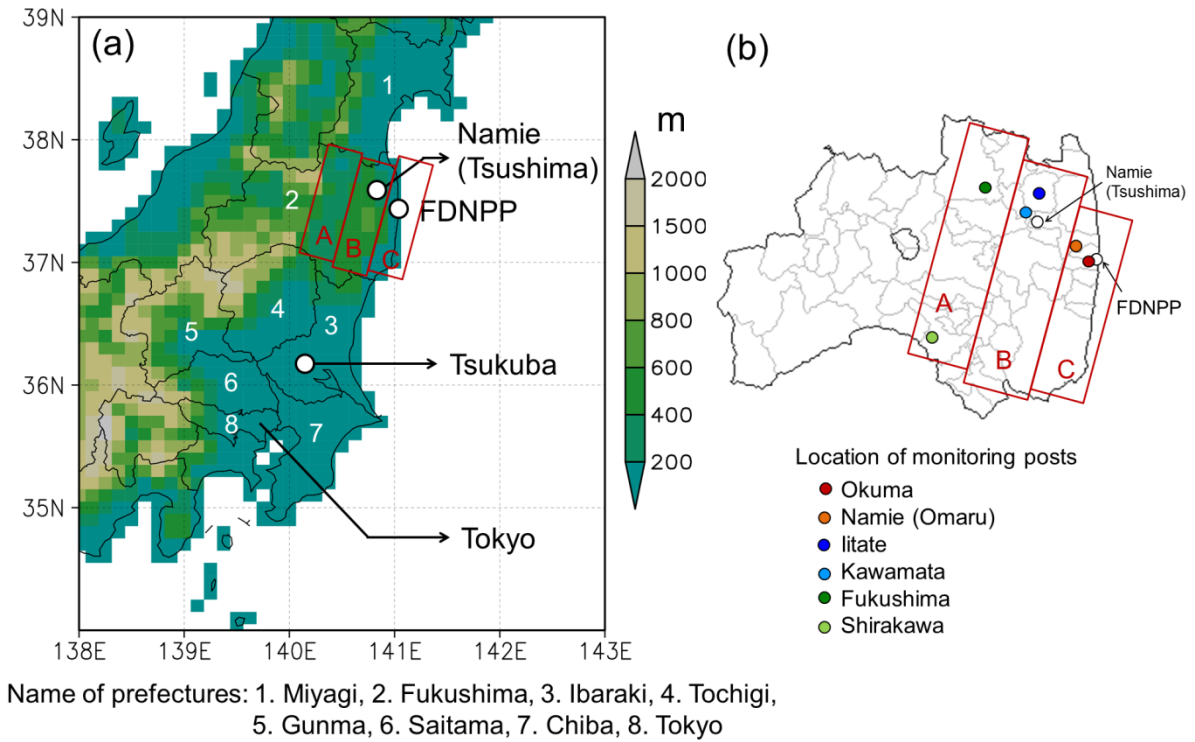
3   Figure 1. (a) The model domain showing the model terrestrial elevation, observation sites, and

4   other locations described in the study. The linear distances from FDNPP to Namie (Tsushima

5   district, Namie town), Tsukuba and Tokyo are approximately 30 km, 170 km, and 220 km,

6   respectively. The numbers denote prefectures: 1. Miyagi, 2. Fukushima, 3. Ibaraki, 4. Tochigi,

7   5. Gunma, 6. Saitama, 7. Chiba, and 8. Tokyo. (b) Fukushima prefecture and (colored circles)

8   the locations (village, town, or city name) of monitoring posts used in this study (see Fig. C1).

9   The letters in both (a) and (b) denote the name of the area based on geographical features: A.

10 Nakadori valley, B. Abukuma highland, and C. Hamadori coastal area.
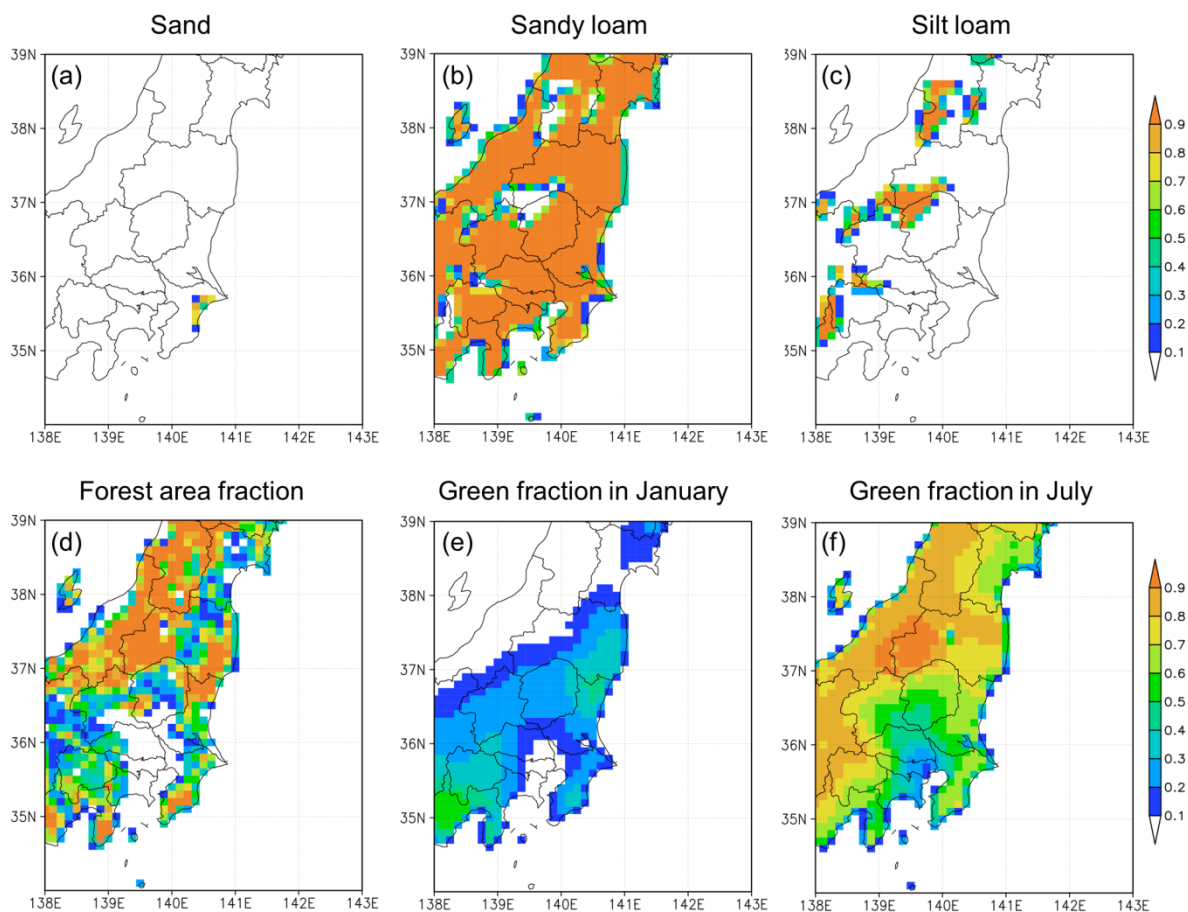
2 Figure 2. The areal fractions of (a)-(c) soil texture and (d)-(f) land use category used for the

3 boundary conditions of the simulation.
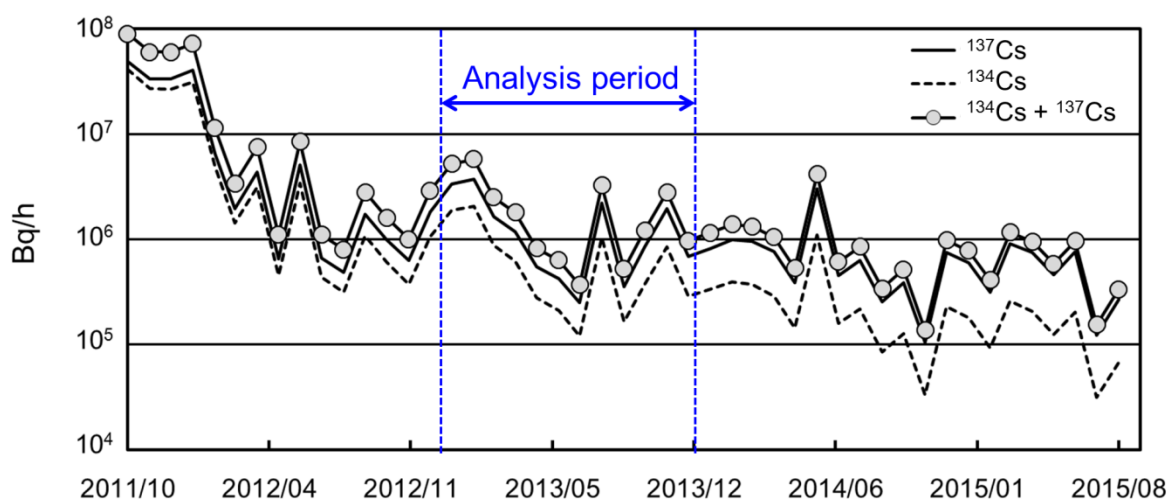
6 Figure 3. Monthly mean emission flux of radiocesium released from the reactor buildings of

7 FDNPP from October 2011 to August 2015 as estimated by TEPCO (TEPCO, 2012-2015).
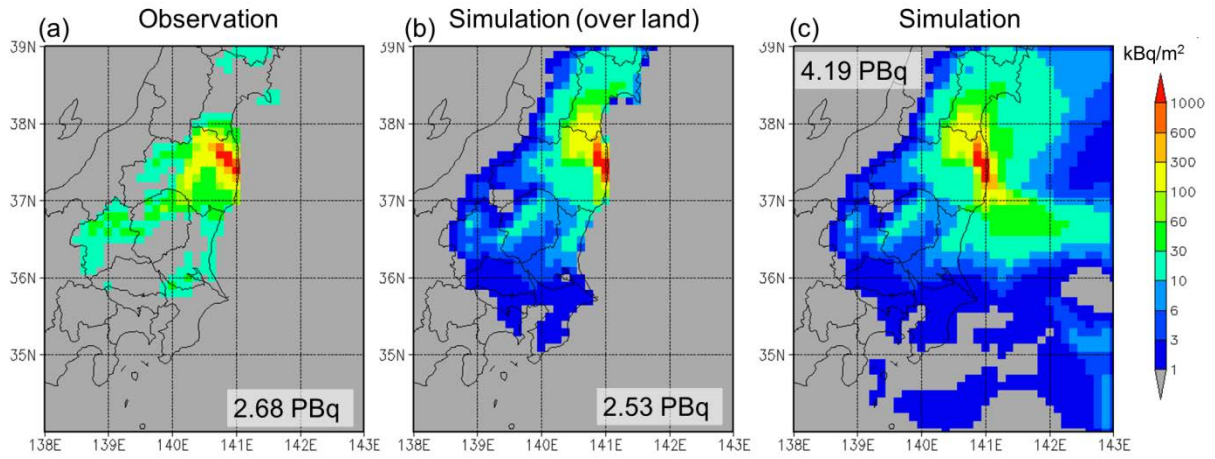
2 Figure 4. (a) Aircraft observation and (b), (c) simulation of ^{137}Cs deposition depicted (b) only

3 over land and (c) for the whole domain (kBq/m^2). The observation was interpolated to the

4 model grid (Δlongitude = 0.125° and Δlatitude = 0.1°). A decay correction for the observation

5 was made for March - May 2012, varied depending on the region. The simulation provided a

6 cumulative value from March 12 to April 1, 2011. The total activities are presented as

7 numbers. The color scales are the same for (a) – (c) but observed values are not depicted

8 below the detection limit, 10 kBq/m^2. The deposition parameters of the simulation in the

9 figure are E_c = 0.04 and v_d = 0.1 cm/s.
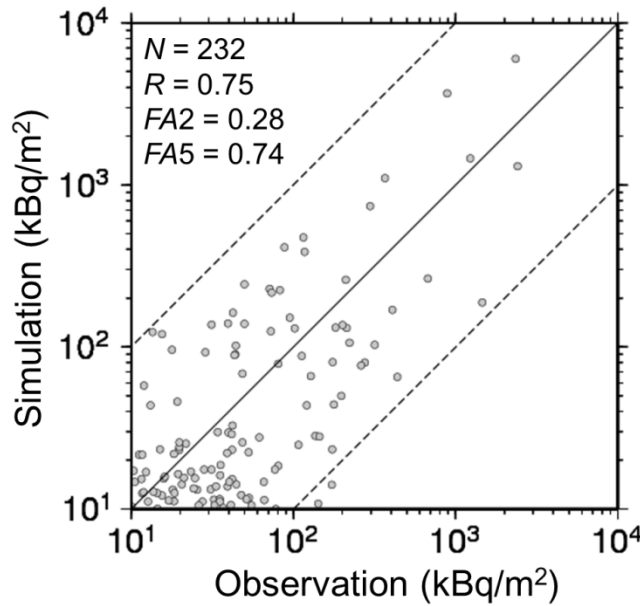
11 Figure 5. Scatterplot between the observational data and the simulation results for ^{137}Cs

12 deposition (kBq/m^2). The deposition parameters of the simulation in the figure are E_c = 0.04

13 and v_d = 0.1 cm/s. N indicates the number of samples, and the statistical measures R, $FA2$, and

14 $FA5$ are described in Table 2.
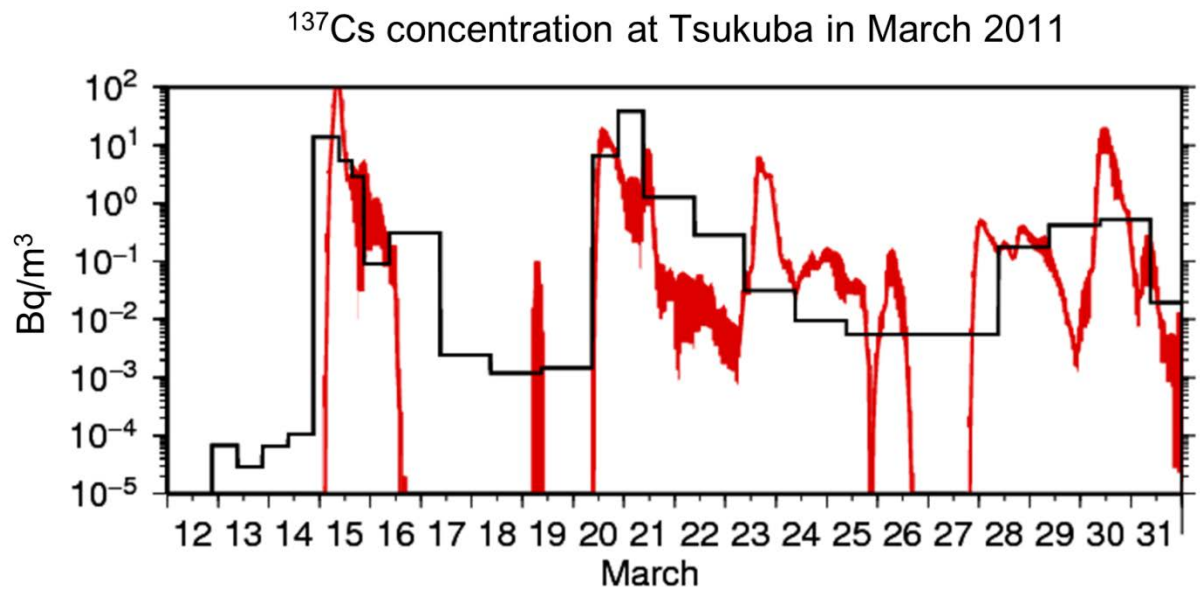
2   Figure 6. Time series of the surface activity concentration of (black) observed and (red)

3   simulated ^{137}Cs concentrations at Tsukuba from March 12 to April 1, 2011 (Bq/m^3). The red

4   shaded areas indicate the range of ^{137}Cs concentrations obtained when the simulations were

5   run using the optimized parameter ranges E_c = 0.03 – 0.05 and v_d = 0.05 – 0.1 cm/s.
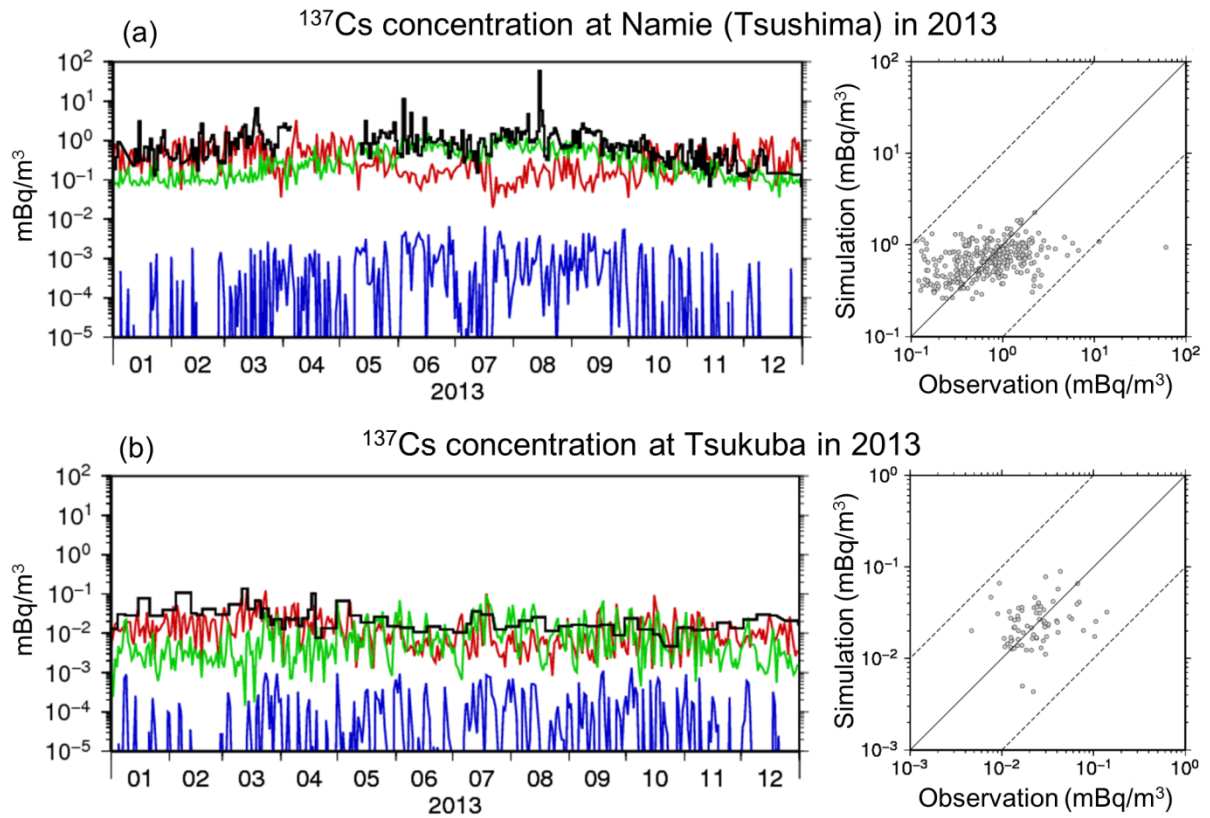
Figure 7. Time series of the surface air concentration of (black) observed ^{137}Cs and (colors) simulated daily ^{137}Cs levels on the left and scatterplots between observed and simulated total (=sum of colors) ^{137}Cs at (a) Namie and (b) Tsukuba. The colored lines indicate simulated ^{137}Cs concentrations due to (red) re-suspension from soil using the scheme given in Ishizuka et al. (2016) (five times), (green) re-suspension from forest with a re-suspension rate of 10^{-7} /h, and (blue) emission from the FDNPP reactor buildings with a constant emission rate of 10^6 Bq/h. The deposition parameters of the simulation in the figure are $E_c = 0.04$ and $v_d = 0.1$ cm/s.
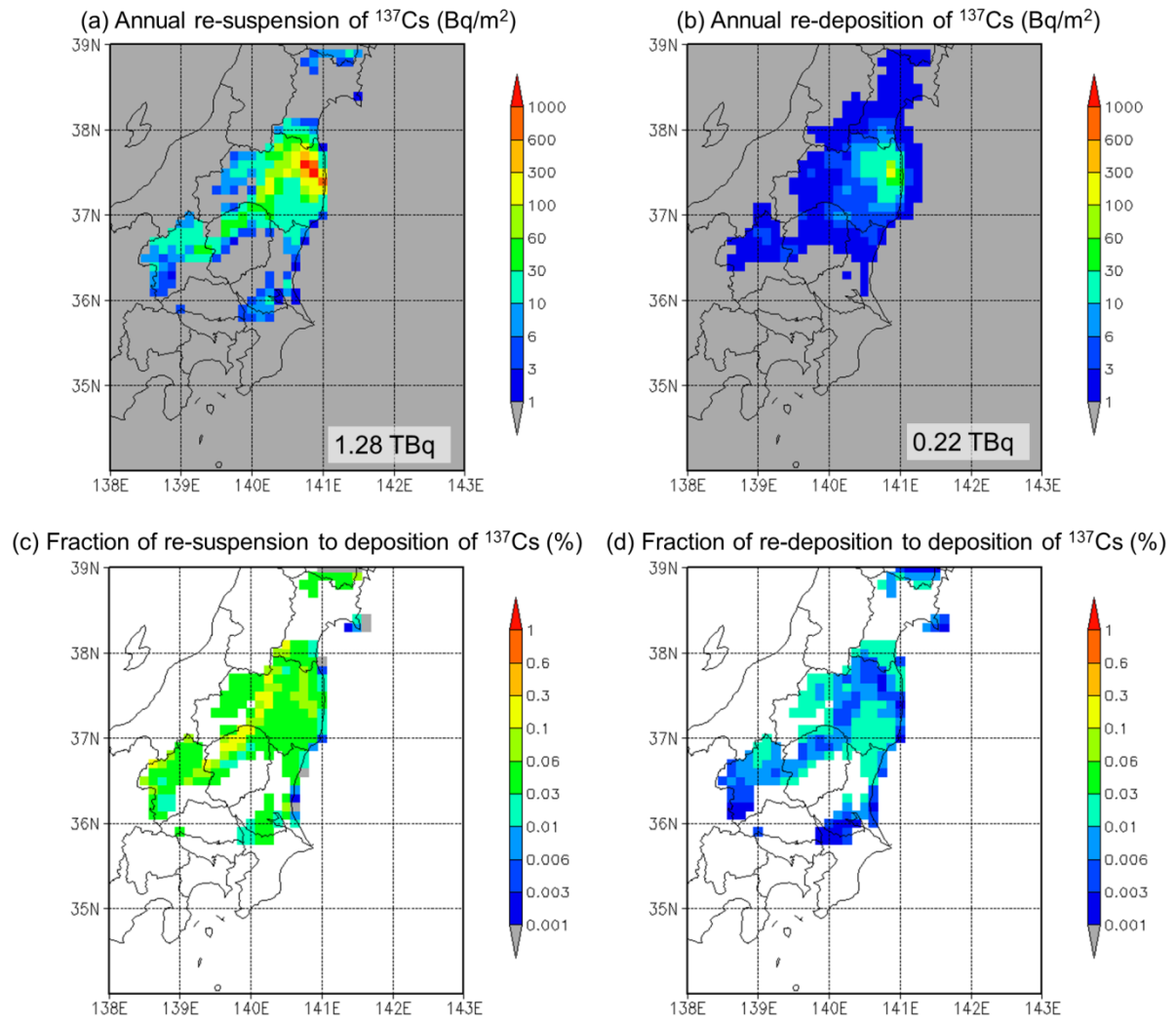
Figure 8. Annual total amounts of (a) the re-suspension and (b) the re-deposition of ^{137}Cs. The total activities are presented as numbers. Fractions of the re-suspension and the re-deposition to the observed ^{137}Cs deposited amounts are also shown in (c) and (d), respectively. The deposition parameters of the simulation in the figure are $E_c = 0.04$ and $V_d = 0.1$ cm/s.
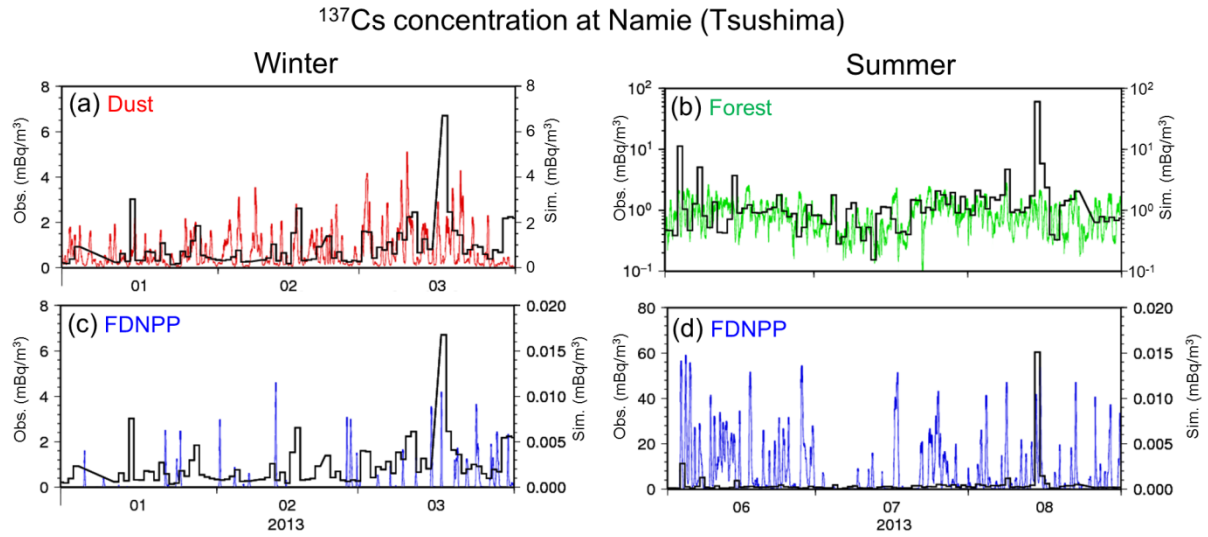
Figure 9. Time series of observed (black) and simulated (colors) ^{137}Cs surface air concentration at Namie (a, c) in winter from January to March and (b, d) in summer from June to August, 2013. The colors of the lines are the same as in Fig. 7 but the time variation is hourly. The shaded areas indicate the range of ^{137}Cs concentrations obtained when the simulations were run using the optimized parameter ranges $E_c = 0.03 - 0.05$ and $v_d = 0.05 - 0.1$ cm/s.
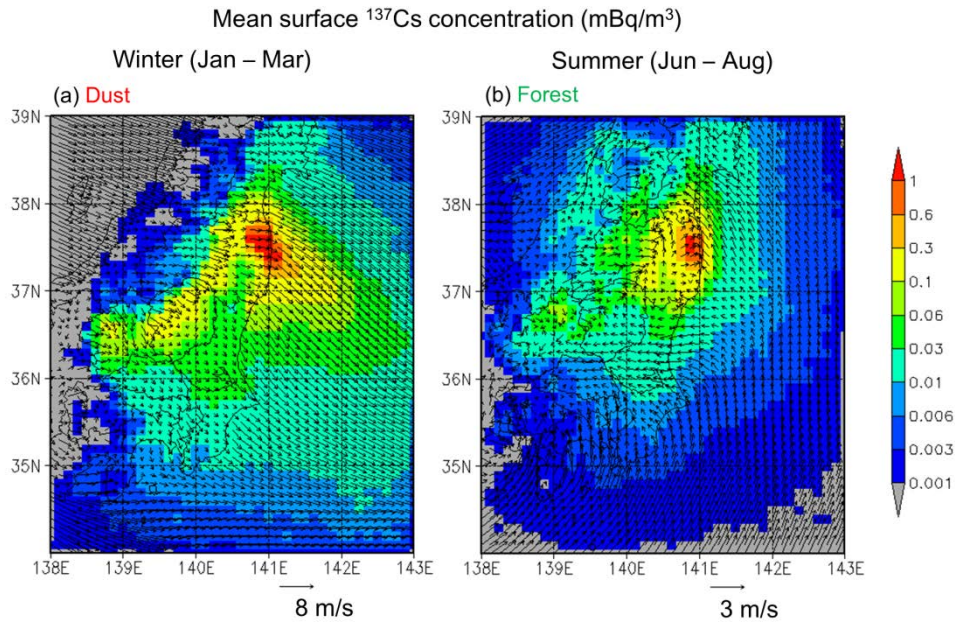
Figure 10. Seasonal mean surface (10 m above ground level) wind vector and ^{137}Cs surface concentration (a) due to dust re-suspension in winter from January to March and (b) due to forest re-suspension in summer from June to August. The deposition parameters of the simulation in the figure are $E_c = 0.04$ and $v_d = 0.1$ cm/s.
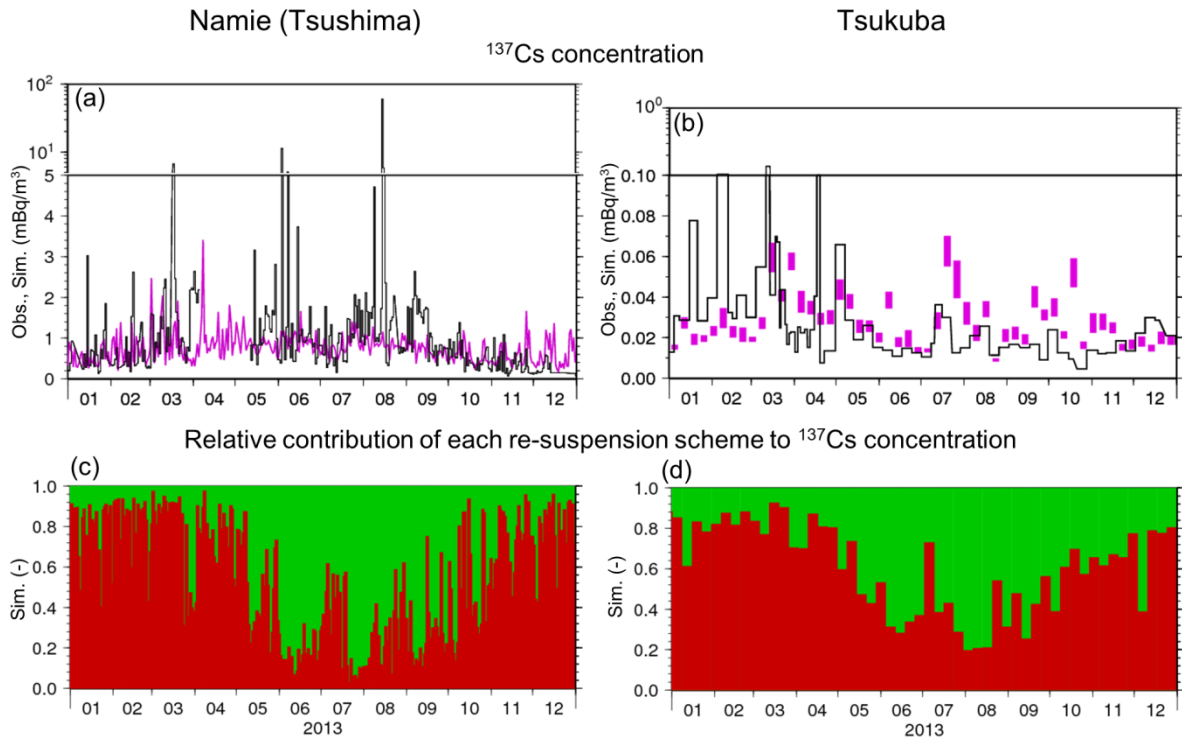
Figure 11. Time series of (a, b) (black) the observed and (purple) the simulated surface ^{137}Cs concentration due to total re-suspension and (c, d) the relative contribution of (red) dust and (green) forest re-suspension to the ^{137}Cs concentration at (a, c) Namie and (b,d) Tsukuba. The shaded areas of (1) and (b) indicate the range of ^{137}Cs concentrations obtained when the simulations were ran using the optimized parameter ranges $E_c = 0.03 - 0.05$ and $v_d = 0.05 - 0.1$ cm/s.
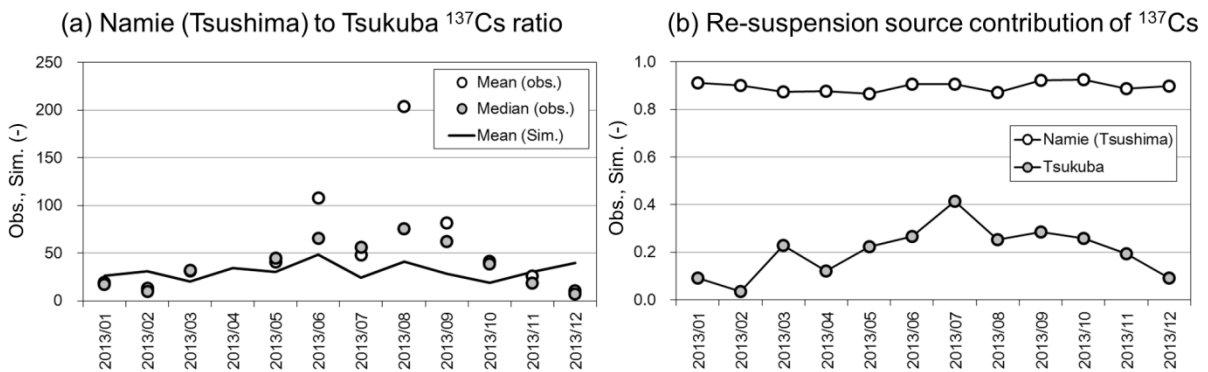
Figure 12. Monthly mean (a) observed mean, observed median and simulated Namie to Tsukuba ^{137}Cs concentration ratio and (b) simulated re-suspension source area (where the observed deposition amount > 300 kBq/m^2) contributions to ^{137}Cs air concentration at Namie and Tsukuba. The deposition parameters of the simulation in the figure are $E_c = 0.04$ and $v_d = 0.1$ cm/s.
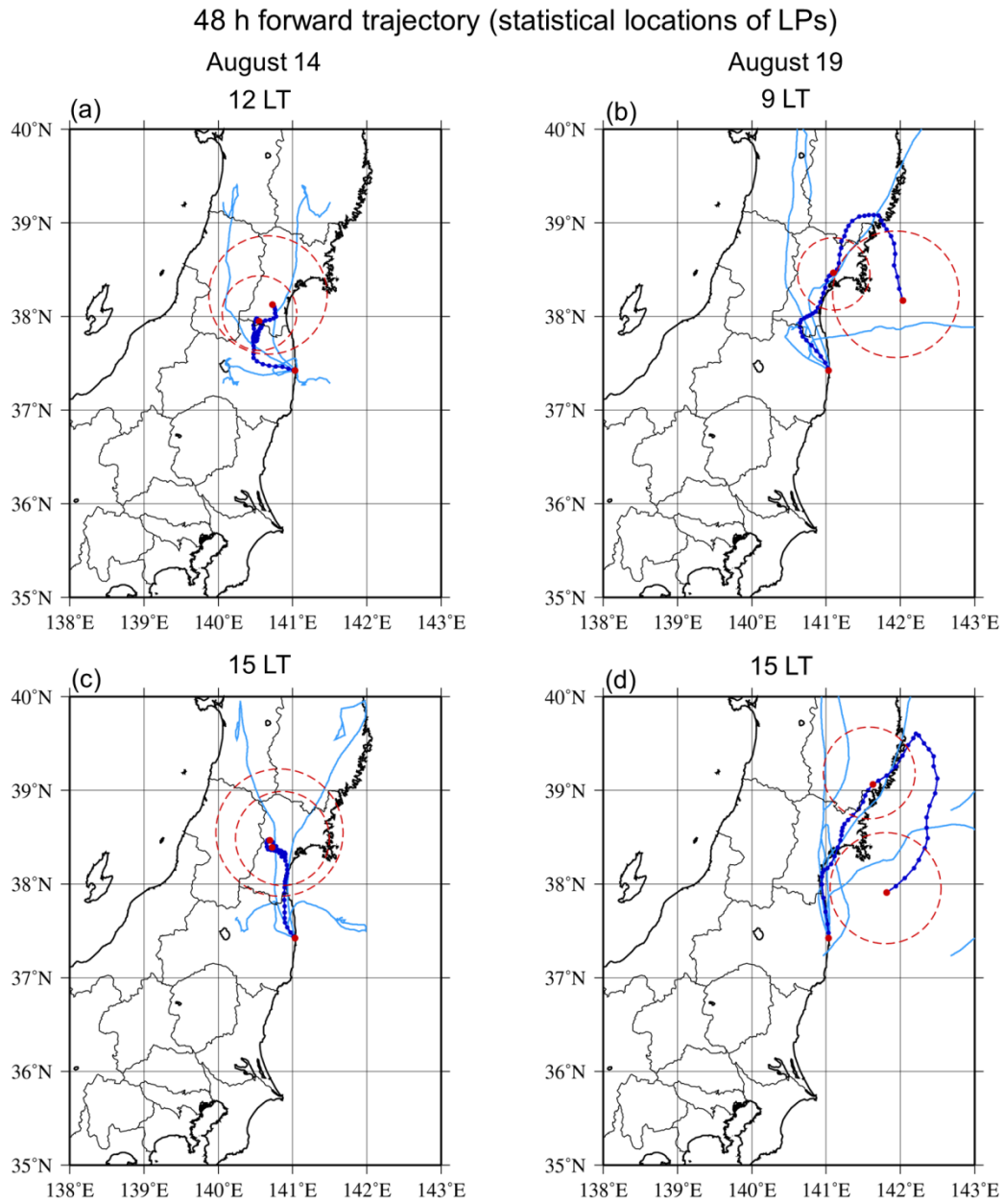
2 Figure 13. 48 h forward trajectory (statistical locations of LPs within 1 km AGL) predicted by

3 the LM starting at (a) 12 LT and (c) 15 LT of August 14 and (b) 9 LT and (d) 15 LT of

4 August 19. Blue lines indicate median locations of LPs at 1 h and 1 d intervals as blue and red

5 dots, respectively. Sky-blue lines indicate 17th and 83rd percentile locations of LPs and red

6 dashed circles indicate areas containing 66% of the LPs.

(a) Daily mean dose rate in a coastal area in Fukushima (Hamadori)
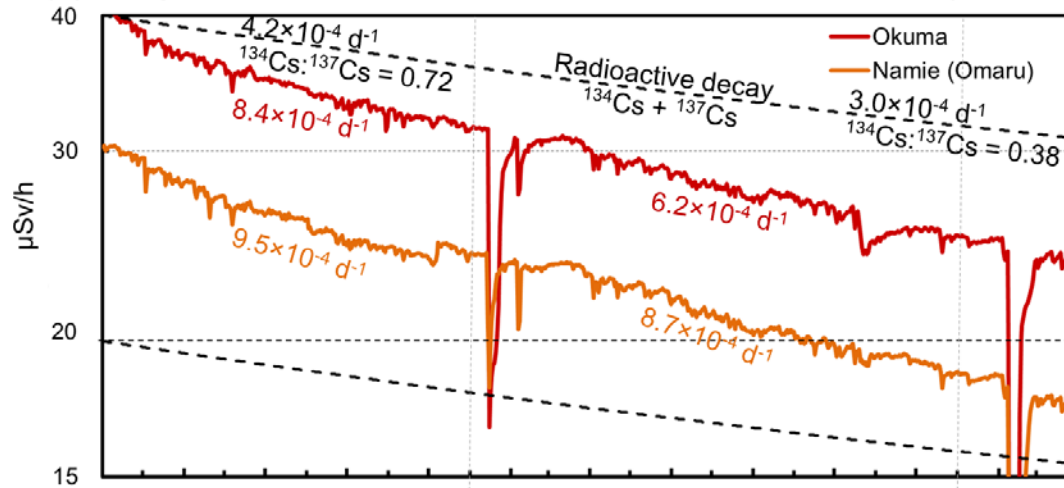
(b) Daily mean dose rate in a mountainous area in Fukushima (Abukuma)
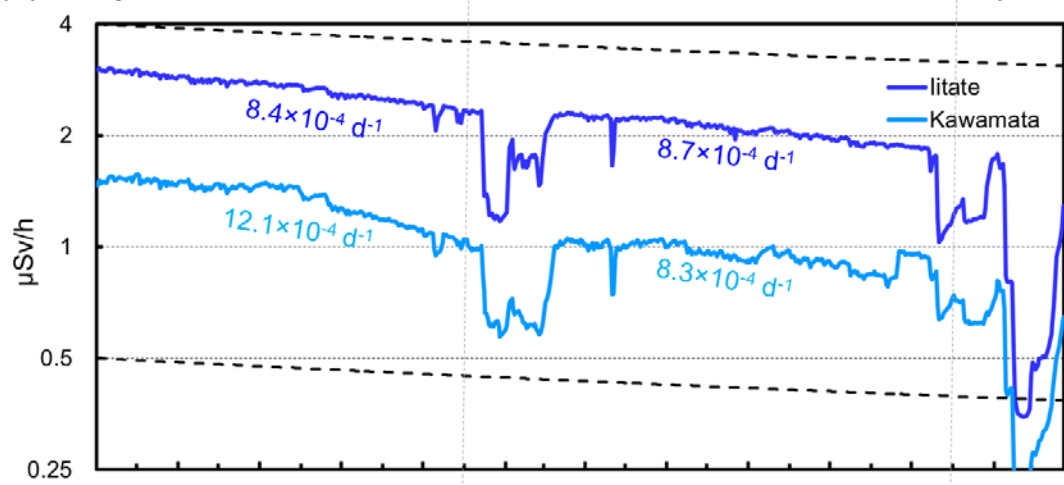
(c) Daily mean dose rate in a valley area in Fukushima (Nakadori)
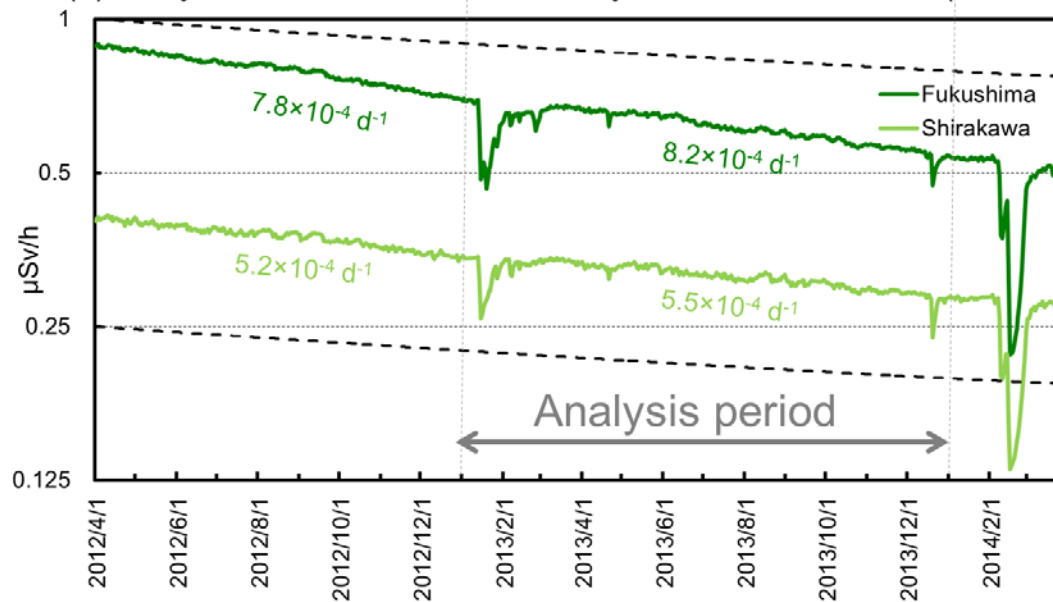
1 Figure 14. Daily mean gamma dose rate at the six monitoring sites: (a) (red) Okuma town and
2 (orange) Namie town (Omaru district) in the coastal area, (b) (blue) Iitate village and (sky
3 blue) Kawamata town in the Abukuma highland area, and (c) (green) Fukushima city and
4 (greenish yellow) Shirakawa city in the Nakadori valley area of Fukushima prefecture as
5 presented in Fig. 1b for two fiscal years (from April 2012 to March 2014). The first-order
6 decreasing rates of the least-square approximation over the period of no snow cover (May to
7 October, 2012 and 2013) is also presented, along with the radioactive decay (^{134}Cs plus ^{137}Cs,
8 by assuming the same amount of activity on March 12, 2011) in April 2012 and March 2013.